

**Effects of Metal Cations and Cyclodextrins on
1,3-Diphenyltriazenes Isomerization and Decomposition**

by

Tingting Xu

A thesis

presented to the University of Waterloo

in fulfillment of the

thesis requirement for the degree of

Master of Science

in

Chemistry

Waterloo, Ontario, Canada, 2009

© Tingting Xu 2009

I hereby declare that I am the sole author of this thesis. This is a true copy of the thesis, including any required final revisions, as accepted by my examiners.

I understand that my thesis may be made electronically available to the public.

Abstract

Triazenes are molecules characterized by having the triazeno group ($-N=N-N<$). They are known as photoactive molecules due to *trans-cis* photoinduced isomerization around the N=N bond. Their nucleophilic character makes them good ligands to metal centers. A study on the potential ability of photochromic organic ligand triazenes to undergo reversible *cis-trans* photoisomerization and, in turn, photoreversible complexation with metal cations was carried out in aqueous solutions. Metal-triazenide complexes are instantaneously formed upon addition of metal cations to *trans*-triazenes dissolved in aqueous solutions. For silver-triazenide and mercury-triazenide complexes, the metal-to-ligand ratios are 1:1 and 1:2, respectively. Unfortunately, target metal-triazenide complexes do not photoisomerize upon 355 nm laser excitation.

Triazenes are also known to be unstable materials under acidic conditions. A study on the effects of cyclodextrins (CDs) on the rate of acid-catalyzed decomposition of 1,3-diphenyl-triazenes was carried out in 2% MeOH aqueous buffer solutions by means of spectroscopic methods. CDs inhibit triazenes decomposition through inclusion complex formation. The inclusion complexes render the guest triazene significantly less basic as a consequence of the less polar nature of the CD cavity (a microsolvant effect). For any given triazene, the inhibition effect is dependent on both the size of the cyclodextrin cavity and the substituents on the cavity rims. Binding constants for 1:1 host:guest complexes increase in the order $\alpha\text{-CD} < \beta\text{-CD} \sim \text{TM-}\beta\text{-CD} < \text{HP-}\beta\text{-CD}$; in the case of $\alpha\text{-CD}$, formation of 2:1 complexes is also observed.

Acknowledgements

First, I would like to give my deepest and most sincere gratefulness to my supervisor Mónica Barra for all she has done for me in the past two years. She is a knowledgeable and careful chemist, a patient and skillful teacher, a strict and fair supervisor, and to me, also a considerate warmhearted friend. She is dedicated to her work and students with great enthusiasm towards chemistry. Her attention to details and endless questions truly helped a lot to force me to think about and understand my project and study. Thanks to her, I have learnt so much in the last two years in both academic and nonacademic aspects.

I would also like to thank my committee members Dr. Mike Chong and Dr. Jean Duhamel for their comments and great suggestions. Thanks to Dr. Xiangdong Fang and Dr. Guy Guillemette as well for generously letting me work on their equipments. Special thanks are given to all the secretaries in the chemistry department, especially to Ms. Cathy van Esch, for their help on various issues.

I would like to acknowledge my wonderful parents deeply and sincerely. Without their endless support, I could not have made it myself today. They inspire me to do my best and always are there for me. I would also like to give my great appreciation to all of my friends either in North America or back in China, their support and carefulness are great treasures to me. I especially thank Angela, Heather and Alice who have made my study and life in Canada so much more enjoyable and colorful.

Last but not least, thanks to the previous group members who synthesized and purified the substrates I used, especially to Atefeh, who shared her data with me.

Dedicated to my dearest and beloved parents.

Table of Contents

List of Tables	viii
List of Schemes	ix
List of Figures	xi
List of Charts	xv
List of Abbreviations, Acronyms and Symbols	xvi
Chapter 1. Introduction	1
1.1 Triazenes	1
1.1.1 <i>Cis-trans</i> isomerization	1
1.1.2 Complexation with metal cations	6
1.1.3 Decomposition	10
1.1.3.1 Photolysis and pyrolysis	10
1.1.3.2 Acid catalyzed decomposition	12
1.2 Cyclodextrins	17
1.2.1 Inclusion complexes	19
1.2.2 Catalysis	23
1.3 Research objectives	26
Chapter 2. Metal-triazene complexes	28
2.1 Results	29
2.1.1 UV-visible absorption spectroscopy	29
2.1.1.1 HDPT	30

2.1.1.2 CH ₃ ODPT.....	34
2.2.1.3 CF ₃ DPT.....	35
2.1.2 Laser flash photolysis (LFP).....	38
2.2 Discussion.....	39
2.3 Conclusions.....	42
Chapter 3. Cyclodextrin effects on the rate of triazenes decomposition	43
3.1 Results.....	44
3.2 Discussion.....	58
3.3 Conclusions.....	68
Chapter 4. Experimental	70
4.1 Reagents and instruments.....	70
4.2 Laser flash photolysis (LFP).....	70
4.3 Preparation of solutions.....	72
4.4 Kinetic data acquisition and processing.....	74
References	76
Appendix. Observed rate constants for acid-catalyzed decomposition of 1,3-diphenyl- triazenes in aqueous solutions	85

List of Tables

Table 1-1. Physical properties of native CDs	19
Table 1-2. Physical properties of some CD derivatives (25°C).....	21
Table 1-3. Dependence of binding constants on solute and cyclodextrin cavity size.....	22
Table 1-4. Binding constants for neutral and ionized forms of various solutes and β -CD ...	23
Table 1-5. Examples of reactions catalyzed or inhibited by CDs.....	26
Table 2-1. Absorption bands of triazenes and of their metal complexes in aqueous solutions.....	39
Table 3-1. Observed rate constants for decomposition of 1,3-diphenyltriazenes in 2% MeOH aqueous solutions at pH 6.16 in the presence of CDs or other glucose additives.....	51
Table 3-2. First order rate coefficients and association equilibrium constants obtained for decomposition of HDPT and CH ₃ ODPT in the presence of CDs.....	61

List of Schemes

Scheme 1-1. <i>Cis-trans</i> isomerization of triazenes	2
Scheme 1-2. Photoreactive system involving azo groups	2
Scheme 1-3. Thermal <i>cis-to-trans</i> isomerization of 1,3-diaryltriazenes	3
Scheme 1-4. Resonance structures of the triazeno group.....	4
Scheme 1-5. <i>Cis-to-trans</i> isomerization of N-(phenylazo)-substituted N-ring heterocycles	5
Scheme 1-6. Photoswitchable equilibria and metal complexation of spiropyran with a divalent metal cation (M^{2+}).....	9
Scheme 1-7. Photolysis and pyrolysis mechanism of triazenes	10
Scheme 1-8. Decomposition mechanism for 1,3-diphenyltriazene	11
Scheme 1-9. Photolysis and pyrolysis mechanism of unsymmetrical triazenes.....	11
Scheme 1-10. Mechanisms for acid-catalyzed decomposition of triazenes: (A) specific acid catalysis; (B) general acid catalysis.....	12
Scheme 1-11. Mechanism for nucleophilic-catalyzed decomposition of triazenes.....	13
Scheme 1-12. Acid catalyzed decomposition of unsymmetrical 1,3-disubstituted triazenes.....	14
Scheme 1-13. General synthetic routes to triazenes	15
Scheme 1-14. Metabolism of antitumor triazenes	16
Scheme 1-15. Covalent catalysis by CDs.....	24
Scheme 1-16. Non-covalent catalysis by CDs.....	25

Scheme 3-1. Specific acid-catalyzed decomposition mechanism for 1,3-diphenyl- triazenes	58
Scheme 3-2. Mechanism for specific acid-catalyzed decomposition of 1,3-diphenyl- triazenes in the presence of CDs	60
Scheme 3-3. Mechanism for specific acid-catalyzed decomposition of 1,3-diphenyl- triazenes in the presence of CDs (with formation of higher order complexes)	63

List of Figures

Figure 1-1. Co-ordination modes of metal-triazene complexes	7
Figure 1-2. Possible metal-triazene complex structures.....	8
Figure 1-3. Typical structure of triazene polymers.....	11
Figure 1-4. Structural requirements of triazene antitumor agents	16
Figure 1-5. Cyclodextrins structure	18
Figure 2-1. Absorption titration spectra of HDPT with Ag^+ in 2% MeOH aqueous solution; top: pH 9, $[\text{HDPT}] = 1.35 \times 10^{-5} \text{ M}$, $[\text{Ag}^+] = 0$ to $1.35 \times 10^{-5} \text{ M}$ (from a to b); bottom: pH 13, $[\text{HDPT}] = 2.62 \times 10^{-5} \text{ M}$, $[\text{Ag}^+] = 0$ to $2.35 \times 10^{-5} \text{ M}$ (from a to b). Inset: corresponding Job's plot.....	30
Figure 2-2. Absorption titration spectra of HDPT ($3.08 \times 10^{-5} \text{ M}$) with Hg^{2+} in 2% MeOH aqueous solution; top: pH 9, $[\text{Hg}^{2+}] = 0$ to $1.26 \times 10^{-5} \text{ M}$ (from a to b to c); bottom: pH 13, $[\text{Hg}^{2+}] = 0$ to $1.67 \times 10^{-5} \text{ M}$ (from a to b). Inset: corresponding Job's plot.....	31
Figure 2-3. Absorption spectra of CH_3ODPT ($1.26 \times 10^{-5} \text{ M}$) in the absence (1) and presence of metal cations (2 , $[\text{Ag}^+] = 1.26 \times 10^{-5} \text{ M}$; 3 , $[\text{Hg}^{2+}] = 0.63 \times 10^{-5} \text{ M}$) in 2% MeOH aqueous solutions at pH 13	35
Figure 2-4. Absorption spectra of CF_3DPT and of its silver complex in 30% THF aqueous solution at pH 9: (a) $[\text{CF}_3\text{DPT}] = 2.82 \times 10^{-5} \text{ M}$; (b) $[\text{CF}_3\text{DPT}] = [\text{Ag}^+] = 1.41 \times 10^{-5} \text{ M}$. Inset: corresponding Job's plot.....	36

Figure 2-5. Absorption titration spectra of CF ₃ DPT with Hg ²⁺ in 30% THF aqueous solutions; top: pH 9, [CF ₃ DPT] = 1.41 × 10 ⁻⁵ M, [Hg ²⁺] = 0 to 2.82 × 10 ⁻⁵ M (from a to b); bottom: pH 13, [CF ₃ DPT] = 2.68 × 10 ⁻⁵ M, [Hg ²⁺] = 0 to 3.22 × 10 ⁻⁵ M (from a to b). Inset: Job's plot.	37
Figure 2-6. Laser induced kinetic trace for HDPT (2.62 × 10 ⁻⁵ M) in 2% MeOH aqueous solution at pH 13. Inset: laser induced kinetic trace for HDPT (2.62 × 10 ⁻⁵ M) in the presence of an equimolar amount of Ag ⁺ in 2% MeOH aqueous solution at pH 9	38
Figure 3-1. Time-resolved absorption spectra for decomposition of HDPT (3.2 × 10 ⁻⁵ M) in 2% MeOH aqueous solution at pH 6.16 (0.05 M phosphate buffer), obtained within 1 min and 45 min (from a to b) after sample preparation. Inset: corresponding spectra obtained within 45 min and 8 h (from b to c) after sample preparation.....	45
Figure 3-2. Absorption-time profile for decomposition of HDPT (3.2 × 10 ⁻⁵) M in 2% MeOH aqueous solution at pH 6.16 (0.05 M phosphate buffer) monitored at 350 nm (○) and 263 nm (□). Inset: expanded profiles obtained within first 58 min.....	45
Figure 3-3. Time-resolved absorption spectra for decomposition of HDPT (3.2 × 10 ⁻⁵ M) in the presence of β-CD (7 mM) in 2% MeOH aqueous solution at pH 6.16 (0.05 M phosphate buffer), obtained within 1 min and 1.7 h (from a to b) after sample preparation. Inset: corresponding spectra obtained within 1.7 h and 8.0 h (from b to c) after sample preparation.	46
Figure 3-4: Absorption-time profile for decomposition of HDPT (3.2 × 10 ⁻⁵ M) in the presence of β-CD (7 mM) in 2% MeOH aqueous solution at pH 6.16 (0.05 M phosphate buffer), monitored at 353 nm (○) and 263 nm (□).....	47

Figure 3-5. Time-resolved absorption spectra for decomposition of CH ₃ ODPT (2.9×10^{-5} M) in 2% MeOH aqueous solution at pH 6.16 (0.05 M phosphate buffer), obtained within 1 min and 16 min (from a to b) after sample preparation. Inset: corresponding spectra obtained within 16 min and 7.3 h (from b to c) after sample preparation.....	48
Figure 3-6. Absorption-time profile for decomposition of CH ₃ ODPT (2.9×10^{-5} M) in the presence of β -CD (7 mM) in 2% MeOH aqueous solution at pH 6.16 (0.05 M phosphate buffer), monitored at 353 nm (○) and 263 nm (□). Inset: expanded profiles obtained within first 17 min.....	48
Figure 3-7. Proton dependence of the observed rate constant for acid-induced decomposition of HDPT (○) and CH ₃ ODPT (□) in 2% MeOH aqueous solutions.....	49
Figure 3-8. Proton dependence of the observed rate constant for acid-induced decomposition of CH ₃ ODPT in 2% MeOH aqueous solutions in the presence of varying amounts of β -CD (concentrations given in mM)	50
Figure 3-9. Influence of α -CD concentration on the observed rate constant for acid-induced decomposition of HDPT (○) and CH ₃ ODPT (□) in 2% MeOH aqueous solution at pH 6.16 (0.05 M phosphate buffer).....	52
Figure 3-10. Influence of β -CD concentration on the observed rate constant for acid-induced decomposition of HDPT (○) and CH ₃ ODPT (□) in 2% MeOH aqueous solution at pH 6.16 (0.05 M phosphate buffer).....	52
Figure 3-11. Influence of HP- β -CD concentration on the observed rate constant for acid-induced decomposition of HDPT (○) and CH ₃ ODPT (□) in 2% MeOH aqueous solution at pH 6.16 (0.05 M phosphate buffer).....	53

Figure 3-12. Influence of TM- β -CD concentration on the observed rate constant for acid-induced decomposition of HDPT (○) and CH ₃ ODPT (□) in 2% MeOH aqueous solution at pH 6.16 (0.05 M phosphate buffer).....	53
Figure 3-13. Absorption titration spectra of HDPT (3.8×10^{-5} M) with α -CD (0, 0.5, 1, 2, 7.5, and 21 mM from a to b) in 2% MeOH aqueous solutions at pH 9.98 (0.05 M borax buffer). Inset: normalized spectra for HDPT in the presence of HP- β -CD (0, 0.2, 0.5, 1, and 10 mM from a to b).....	55
Figure 3-14. Absorption titration spectra of CH ₃ ODPT (3.5×10^{-5} M) with α -CD (0, 0.5, 1, 2, 3, 4, 5, 7.5, 10, 13.5, 17 and 21 mM from a to b,) in 2% MeCN aqueous solutions at pH 9.98 (0.05 M borax buffer)	55
Figure 3-15. Induced circular dichroism (top) and absorption (bottom) spectra of HDPT (3.2×10^{-5} M) in the presence of CDs (7 mM): (a) α -CD; (b) β -CD; (c) HP- β -CD; (d) TM- β -CD.....	56
Figure 3-16. Induced circular dichroism titration spectra of HDPT (3×10^{-5} M) with α -CD (0.5, 1, 2, 3, 4, 5, 7.5, 10, 17 and 21 mM, from bottom to top) in 2% MeOH aqueous solutions at pH 9.98 (0.05 M borax buffer).....	57
Figure 4-1. Laser flash photolysis apparatus diagram	71
Figure 4-2. Possible kinetic traces observed with a LFP system.....	72

List of Charts

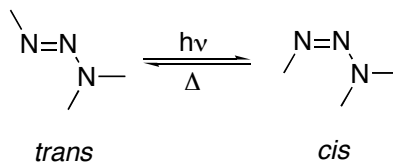
Chart 2-1. Structure and abbreviation of target substrates	28
Chart 3-1. Structure and abbreviation of host molecules	43

List of Abbreviations, Acronyms and Symbols

A	Absorbance
ΔA	Change in absorbance
CD	Cyclodextrin
CF ₃ DPT	1,3-Bis(3-trifluoromethylphenyl)triazene
CH ₃ ODPT	1,3-Bis(4-methoxyphenyl)triazene
COP- β -CD	6 ^A ,6 ^D -Di-C-oxo-6 ^A ,6 ^D -O-(2-oxo-1,3-propanediyl)- β -CD
DM- β -CD	Heptakis(2,6-di-O-methyl)- β -CD
DMSO	Dimethylsulfoxide
Eq.	Equation
HDPT	1,3-Diphenyltriazene
HP- β -CD	Heptakis(2,3,6-tri-O-2-hydroxypropyl)- β -CD
2-HP- β -CD	2-Hydroxypropyl- β -CD
2-HP- γ -CD	2-Hydroxypropyl- γ -CD
ICD	Induced circular dichroism
K_a	Acid dissociation equilibrium constant
k	Rate constant
LASER	Light Amplification by Stimulated Emission of Radiation
LFP	Laser flash photolysis
MC/PMT	Monochromator/Photomultiplier
MeCN	Acetonitrile
MeOH	Methanol
PFD- α -CD	6 ^A ,6 ^D -Di-O-(2-formyl-1,3-propanediyl)- α -CD

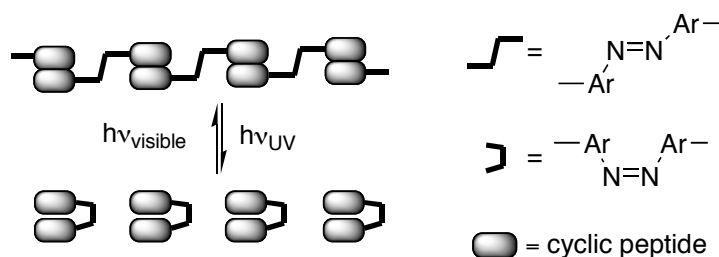
RM- β -CD	Randomly methylated- β -CD
THF	Tetrahydrofuran
TM- β -CD	Heptakis(2,3,6-tri- <i>O</i> -methyl)- β -CD
UV	Ultraviolet
YAG	Yttrium Aluminum Garnet
γ_{H^+}	Proton activity coefficient
λ_{max}	Wavelength of maximum absorbance
μ	Ionic strength

trans isomerization renders triazenes as photochromic compounds and hence, potential photoswitchable materials.



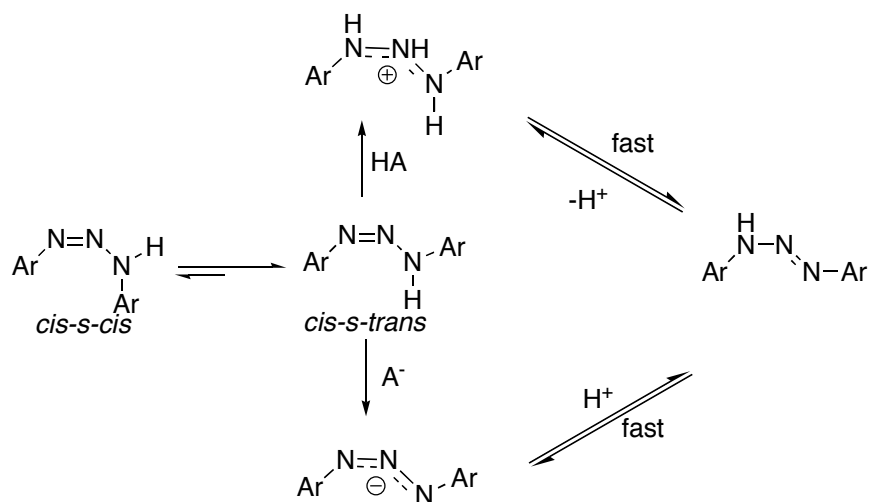
Scheme 1-1. *Cis-trans* isomerization of triazenes

Photoswitchable materials based on double bond *cis-trans* isomerization have been employed in the development of erasable optical recording supports, image processors, laser-addressable devices, light switchable receptors and sensors, and the control of the conformation of biomolecules.⁶ Azobenzenes represent one of the most thoroughly studied N-containing systems with photoswitchable properties.^{7,8} Covalent attachment of azobenzene units to enzymes has allowed protein activity modulation by distorting the protein structure through isomerization around the N=N double bond.⁹ Two cyclic peptides are joined together with an azo group to form a photo reactive molecule; in the thermally preferred *trans* form, the molecules self-assemble via hydrogen-bonding to form an extended network structure, while upon UV irradiation, the molecules spontaneously disrupt the network structure through self-association (Scheme 1-2).⁹



Scheme 1-2. Photoreactive system involving azo groups

Triazenes display photoisomerization similarly to that of azo compounds, and thus may have similar applications.⁶ In order to make use of these materials, it is very important to know how the isomerization occurs. Our group has focused on mechanistic studies of the thermal *cis*-to-*trans* isomerization of 1,3-diaryltriazenes in aqueous media for a couple of years, and suggested an acid/base-catalyzed mechanism as shown in Scheme 1-3.¹⁰⁻¹⁴

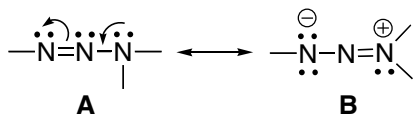


Scheme 1-3. Thermal *cis*-to-*trans* isomerization of 1,3-diaryltriazenes

Cis triazenes are obtained by laser photoexcitation of *trans* forms at 355 nm. For symmetrical disubstituted triazenes, the mechanism is as shown in Scheme 1-3. At $6 < \text{pH} < 8$ (due to the instability of triazenes in acidic conditions, measurements at $\text{pH} < 6$ aqueous solutions were not able to be carried out), rate-determining proton transfer to the $N^1=N^2$ double bond gives a resonance-stabilized cation, which then loses a proton from the position that renders the thermodynamically more stable *trans*-isomer.^{10,11} At $8 < \text{pH} < 11$, the *cis*-to-*trans* isomerization follows a base catalyzed mechanism. The rate-determining base-promoted ionization of the amino N gives a resonance-stabilized

anion, which then combines with a proton at the position that leads to the thermodynamically more stable *trans*-triazene.^{10,11} In all cases, the catalytic rate coefficients are found to increase as the pK_a difference between the triazene and Brønsted catalyst also increases.¹¹ Thus, with increasing electron-donating character of the *para* substituent, acid catalysis becomes more prominent, while with increasing electron-withdrawing character of the *para* substituent, base catalysis becomes more important.^{11,13} In the case of unsymmetrically disubstituted 1,3-diaryltriazenes, due to the existence of distinguishable tautomeric isomers, two pairs of *cis*-isomers are obtained from the excitation of the *trans* isomers. These two pairs of *cis*-isomers undergo isomerization independently of one another, each pair following the mechanism showed in Scheme 1-3.^{13,14}

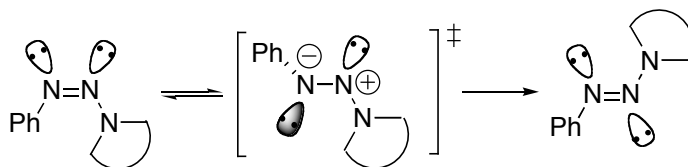
Both acid and base catalyzed isomerizations involve a fast interconversion between two rotamers of *cis*-triazenes, *i.e.*, the *cis-s-cis* and *cis-s-trans* isomeric forms (Scheme 1-3). The interconversion occurs via N²-N³ bond rotation, which has a relatively high free energy barrier due to the partial double bond character resulting from a 1,3-dipolar form (Scheme 1-4).¹⁵ It is not hard to see that only the *cis-s-trans* form can lead to N¹=N² double bond isomerization; protonation or deprotonation of the *cis-s-cis* form does not lead to any change in N¹=N² double bond configuration.



Scheme 1-4. Resonance structures of the triazeno group

In NaOH solutions (pH > 11), the interconversion of *cis* rotamers via hindered rotation around the N²-N³ bond is the rate-controlling step.^{10,11} The rate of this process is found to be more susceptible to the electronic character of the aryl group bonded to N¹ than of that attached to N³,¹⁴ and to decrease with decreasing solvent polarity, implying an increase in dipole moment on rotation from the ground state to the transition state.^{11,12}

The most recently published work focused on the mechanism of *cis*-to-*trans* isomerization of N-(phenylazo)-substituted N-ring heterocycles.¹⁶ It is shown that, in organic solvents, the observed first-order rate constants for thermal *cis*-to-*trans* isomerization increase with increasing electron-withdrawing character of the *para* substituent on the phenyl ring, larger amine rings, and increasing solvent polarity. These observed trends are consistent with the geometrical isomerization taking place through rotation around the N=N double bond via a polarized transition state (Scheme 1-5).¹⁶ The ability of the phenyl and cycloamine rings to stabilize, respectively, the negative and the positive charges in the polarized transition state as well as in the resonance form **B** (Scheme 1-4) of the ground state *cis*-triazene, will influence the rotational energy barrier and hence, the reaction rate. An electron withdrawing group on the phenyl ring and a larger cycloamine ring will not only stabilize the polar transition state but also lead to a decrease in the N1=N2 bond order (by increasing the contribution of resonance form **B** in the ground state *cis*-triazene), thus making the isomerization reaction to go faster.¹⁶



Scheme 1-5. *Cis*-to-*trans* isomerization of N-(phenylazo)-substituted N-ring heterocycles

1.1.2 Complexation with metal cations

The nucleophilic character of triazenes makes them good ligands to complex with metal centers with various arrangements of triazenide-metal bonds.^{17,18} The study of transition metal complexes containing triazenide ligands has increased greatly in the past few years due to their various applications. Suitable systems may display novel catalytic properties; for instance, a polymer supported Pd(II)-triazene complex has been reported to have good activity in both Sonogashira and Suzuki reactions.¹⁹ In addition, some triazenide ligands can stabilize unusual oxidation states of metals in dimeric complexes. For example, 1,3-bis(aryl)triazenide ligands bearing Lewis basic groups in the *ortho*-positions appear to facilitate the reduction of Pd(II) to the uncommon Pd(I) and to stabilize Pd in the +1 oxidation state.²⁰ Moreover, a popular analytical application of triazenes is in the spectrophotometric determination of metal cations. For example, 1-(4-nitrophenyl)-3-(2-quinolyl)triazene has been reported as an extremely sensitive reagent for determination of mercury in water;²¹ hydroxytriazenes have been widely used for the extraction and subsequent photometric determination of copper, palladium, iron, cobalt, nickel and molybdenum;²² *m*-nitrophenylazo-2-aminothiazole has been used for the determination of trace impurity silver in an anticancer drug and in chemical samples and for the measurement of the solubility product of AgCl;²³ and dibromo-6-carboxy-benzenediazoaminoazobenzene can be used for determination of trace amounts of silver in waste-water.²⁴

Triazenes are used as precursors for triazenide complexes, in which the metals take the place of the amino H; only four metals (Ir, Rh, Ru, and Os) can form complexes with triazenes without replacing the amino H.²⁵⁻²⁷ Not a single article about trisubstituted

triazenes forming complexes with metals could be found. The three most fundamental coordination modes of metal-triazenide complexes have been identified as: (a) monodentate, (b) chelate and (c) bridging modes (Figure 1-1).¹⁸

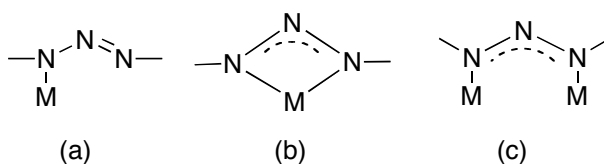


Figure 1-1. Co-ordination modes of metal-triazenide complexes

It has been reported that binuclear-bridged bonding is more likely to be present in transition metal complexes.²⁸ The triazene complexes of Ni (II), Cu (II) and Pd (II) are isomorphous (structure **a** in Figure 1-2), while Cu (I), Ag (I) and Pd (I) complexes are more likely to arrange as represented by structure **b** in Figure 1-2.^{20,28-31} The dark green Cu (II)-1,3-diphenyltriazene complex is extremely unstable and decomposes very quickly to the orange-brown Cu (I)-1,3-diphenyltriazene complex, releasing N₂, aryl radicals and aryl amine radicals through auto-reduction.³² Interestingly, in Ag (I) triazene complexes, the Ag atoms are found to form zigzag polymeric chains while the bridging triazenido ligands are arranged alternately above and below the Ag chain (structure **c**, Figure 1-2).³⁰ By far, the most interesting feature of these kinds of complexes is the possible metal-metal bonding due to the close metal-metal distances.^{29,30}

Depending on the ligands originally present in Pd (II) and Pt (II) complexes, triazenes can form new complexes either by a chelating mode (Figure 1-1(b)) or by a bridging mode (Figure 1-1(c)).³³ Mercury (II)-triazenide complexes may have different structures depending on which mercury salt was used during the synthetic process.³⁴ When HgCl₂

or HgBr_2 is used, structure **d** (Figure 1-2) in which the central mercury is 4-valent is the resulting structure; when acetate or nitrate salts are used, the 4-valent mercury center is maintained as in structure **e** (Figure 1-2).³⁴ Group III metals can form complexes with triazenes as well. An interesting observation is that a complex with a tris-chelate structure (**f**, Figure 1-2) was the only product isolated from the reaction between 1,3-diphenyl-triazene and AlMe_3 ; the gallium and indium analogues can be obtained in a similar manner to the aluminum complex, resulting in the same tris-chelate structure.³⁵

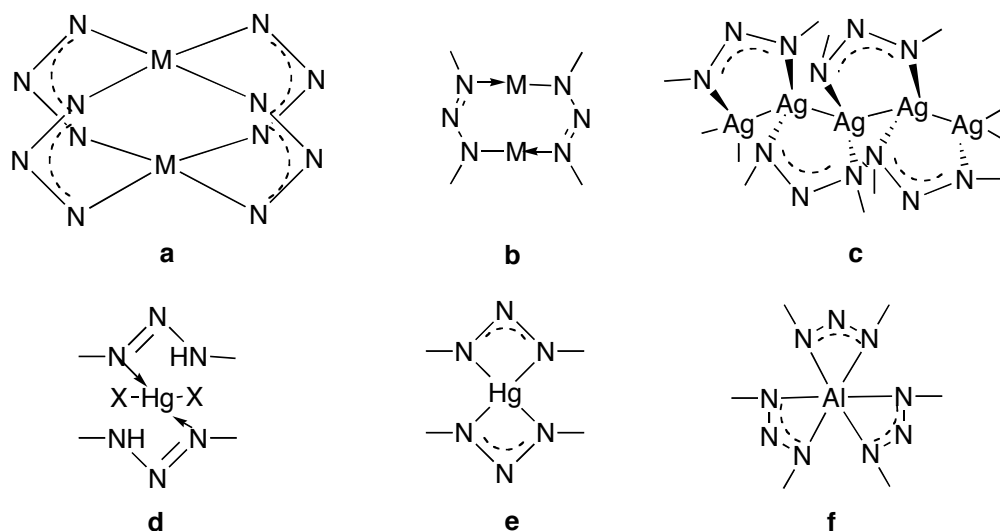
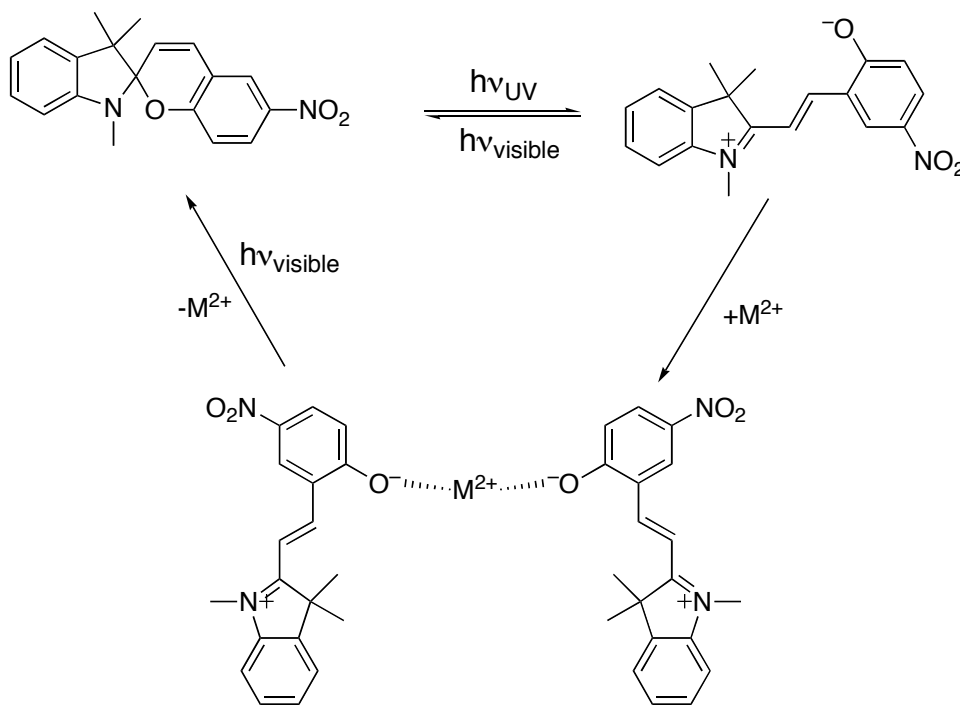


Figure 1-2. Possible metal-triazene complex structures

Metal complexes involving photochromic moieties and coordination compounds have been found to display unique electronic, magnetic and optical properties.³⁶ A study on spiropyrans has showed their promising application in surface-based photoswitchable chemical sensors due to the fact that spiropyrans can be switched between two states (“on” and “off”) through a ring opening reaction that is induced by photoexcitation.³⁷ One state is an uncharged, colorless, passive spiropyran form; after UV illumination, it

converts to a zwitterionic, highly colored active merocyanine form which complexes with metals (Scheme 1-6).³⁷ The “on” state is stabilized in solvents of high polarity, thereby continuous visible irradiation is needed for the metal complex to transform back to the “off” state.³⁷ Bearing in mind both the photochromic and metal complexing abilities of triazenes, if only one isomeric form of triazenes (*trans* form) has binding ability to metal cations and the other form (*cis* isomer) is passive, in principle, it may be possible for triazene-metal complexes to exhibit a similar “on” and “off” behavior through photoisomerization; one of the objectives indeed of this thesis is to explore the possibility of triazene-metal complexes to function as photoswitchable materials.



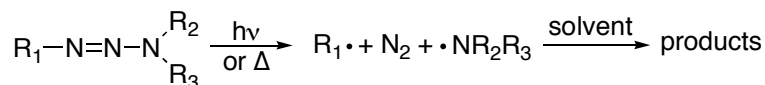
Scheme 1-6. Photoswitchable equilibria and metal complexation of spiropyran with a divalent metal cation (M^{2+}).

1.1.3 Decomposition

1.1.3.1 Photolysis and pyrolysis

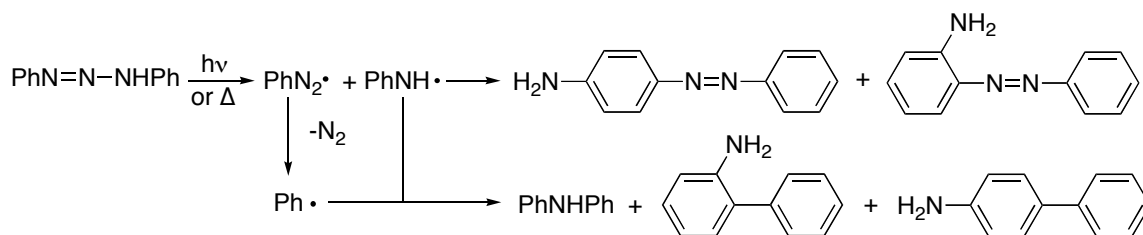
As already mentioned, triazene $\text{HN}=\text{N}-\text{NH}_2$ is very unstable; it undergoes rapid decomposition by cleavage of the N^2-N^3 bond even at room temperature while its derivatives (substituted triazenes) usually have much greater stability, particularly when aryl substituents are present.^{1a} For example, some of the 1-aryl-3,3-dialkyltriazenes can be distilled at temperatures as high as 150°C . However, most triazenes decompose below 300°C .^{1a}

Triazenes decomposition can be induced not only by heat but also upon UV light exposure. In both cases, decomposition progresses through homolytic N^2-N^3 bond cleavage of the triazeno group. The mechanism for photolysis and pyrolysis of triazenes can be represented as shown in Scheme 1-7.^{5,38-40}

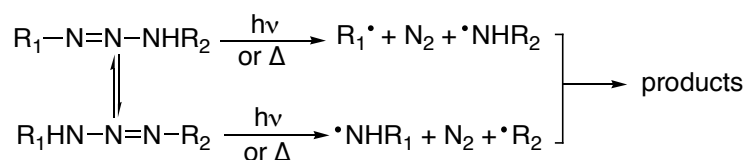


Scheme 1-7. Photolysis and pyrolysis mechanism of triazenes

The decomposition mechanism for 1,3-diphenyltriazenes (Scheme 1-8), which also applies to 1,3-diaryltriazenes, is worth mentioning because many phenyl products can be obtained from the decomposition of different 1,3-diaryltriazenes.⁵ In the case of unsymmetrical 1,3-disubstituted triazenes, the mechanism becomes more complex due to substrate tautomerization, resulting in additional radical intermediates that can undergo either recombination or degradation to give various product species (Scheme 1-9).³⁸



Scheme 1-8. Decomposition mechanism for 1,3-diphenyltriazene



Scheme 1-9. Photolysis and pyrolysis mechanism of unsymmetrical triazenes

The ability of triazenes to undergo homolytic N^2-N^3 bond cleavage (and consequently, to release N_2 gas) makes them suitable materials in polymer chemistry, especially in polymer laser ablation.^{41,42} Figure 1-3 shows a typical structure for triazene polymers, the absorption maximum of which can be tuned from 260 nm to 360 nm by varying the “X” moiety in the polymer.⁴¹ In fact, triazene polymers show one of the best ablation performances on exposure at 308 nm (the most common irradiation wavelength applied in industry).⁴²

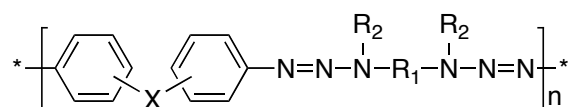
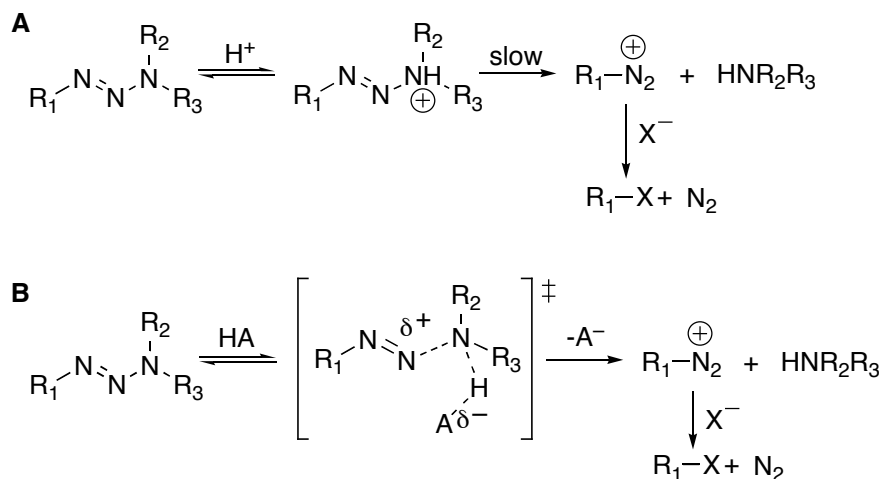


Figure 1-3. Typical structure of triazene polymers

1.1.3.2 Acid catalyzed decomposition

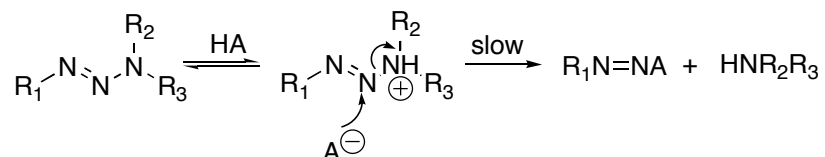
Triazenes decompose in the presence of acids to amines and diazonium ions intermediates, which subsequently lead to N_2 gas and substitution products. Two decomposition mechanisms commonly accepted are: (1) specific acid catalysis (which involves a fast reversible protonation at the N^3 atom followed by rate-determining heterolysis of the protonated species to diazonium ions and amines, Scheme 1-10 A)⁴³⁻⁴⁵ and (2) general acid catalysis (which involves simultaneous protonation of the N^3 atom and splitting of the N^2 - N^3 bond, Scheme 1-10 B).⁴⁶⁻⁴⁹ The rate of a specific acid catalyzed reaction is proportional to proton concentration, while that of a general acid catalysis is proportional to the concentration of each of the acidic species present in the solution.^{50a} Thus, a notable experimental difference between these two mechanisms is that at constant proton concentration, the observed rate constant of a specific acid catalysis does not change by varying the buffer concentration, while that of a general acid catalysis is proportional to buffer concentration.^{50a}



Scheme 1-10. Mechanisms for acid-catalyzed decomposition of triazenes:

(A) specific acid catalysis; (B) general acid catalysis

Another, less common, decomposition pathway for triazenes involves fast protonation at the N³ atom followed by rate-limiting nucleophilic attack (Scheme 1-11).⁴³ The rate for this reaction does respond to proton and buffer concentrations in the same manner as in a general acid catalyzed system. Measurement of the kinetic solvent isotope effect (KSIE), *i.e.*, the ratio between the reaction rate in H₂O and that in D₂O, can help to distinguish between these two different reaction pathways. For general acid catalysis, proton transfer is the rate-limiting process. Since H-A bond is weaker than D-A bond, the reaction in H₂O will be faster than in D₂O; thus, one should expect a KSIE larger than 1. On the other hand, for nucleophilic catalysis (as well as specific acid catalysis) proton transfer takes place in a pre-equilibrium step, not the rate-limiting step. Such an equilibrium will be driven to the right when H₂O is substituted by D₂O, since D₃O⁺ is a stronger acid than H₃O⁺; thus, one should expect a KSIE smaller than 1.^{50a}

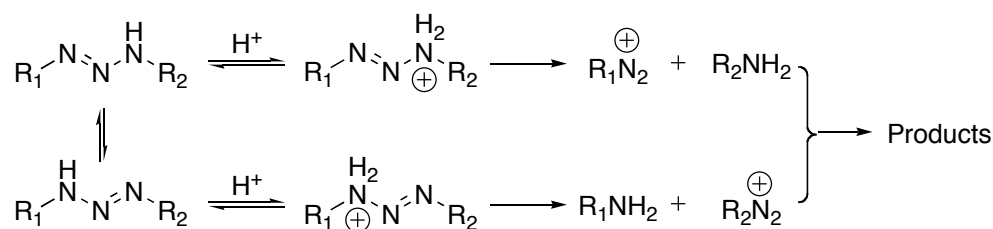


Scheme 1-11. Mechanism for nucleophilic-catalyzed decomposition of triazenes

All of the above mechanisms show protonation at the N³ atom only, while in fact a proton can attach to any of the three nitrogen atoms in the triazeno group.^{51,52} According to quantum-chemical calculations of heats of formation of the different protonation intermediates, protonation at N¹ and N³ atoms are competitive while both of them are more favored than protonation at N².⁵² An *ab initio* molecular orbital calculation study

shows that although protonation at N¹ is preferred, it is protonation at N³ that results in the N²-N³ bond scission, which is consistent with the kinetic experimental data.⁵¹

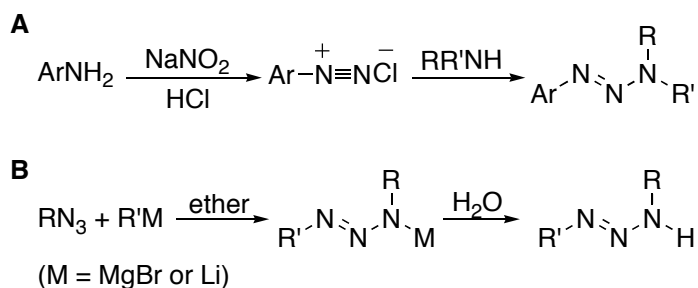
As in the case of pyrolysis and photolysis, acid catalyzed decomposition of unsymmetrical 1,3-disubstituted triazenes becomes more complex due to substrate tautomerization (Scheme 1-12).¹⁷ Both tautomers can undergo decomposition through protonation at the N³ atom, resulting in different decomposition intermediates and product species; corresponding product distribution is controlled by the difference in standard free energies of the two possible transition states that lead to diazonium ions.⁴⁴



Scheme 1-12. Acid catalyzed decomposition of unsymmetrical 1,3-disubstituted triazenes

The acid-induced decomposition of 1,3-diphenyltriazenes has been reported to be solvent sensitive; the overall trend is that the decomposition rate decreases with decreasing solvent polarity.^{46,47,53} Encapsulation of guest molecules into macrocycles can change the microenvironment of the guest molecules, hence altering the properties of the guest species, such as solubility and reactivity. Indeed, the other objective of this thesis is to investigate the effects of encapsulation of triazenes into cyclodextrins, one of the most popular host molecules (Section 1.2), on the acid-induced decomposition of 1,3-diphenyltriazenes.

It should be pointed out here that the acid catalyzed decomposition pathways shown above are just the opposite to one of the synthetic routes to triazenes: N-coupling of diazonium ions with amines (Scheme 1-13 A).^{17,54} This pathway is commonly used in the synthesis of aromatic triazenes, in which anilines are typically treated with nitrite ion under acidic conditions to form aryl diazonium salts, which are then quenched with a primary or secondary amine to provide the desired triazene. On the other hand, alkyl-substituted triazenes are typically obtained from the reaction of an alkyl azide with the appropriate Grignard or alkyl lithium reagent (Scheme 1-13 B).^{17,54}



Scheme 1-13. General synthetic routes to triazenes

Due to the fact that triazenes can be easily synthesized from and readily decompose to amines and diazonium ions, which are widely used in organic synthesis, triazenes have become very useful not only as protecting groups for amines but also as *in situ* sources of diazonium ions (which in turn undergo rapid fragmentation to the very stable N₂ molecule and highly reactive cationic intermediates).⁵⁴⁻⁵⁶ The use of triazenes in organic synthesis may allow to achieve product selectivity that other reactions cannot.⁵⁴ For example, synthesis of primary aniline derivatives by lithiation has been generally limited to those producing *ortho*-substituted ones; selective synthesis of *ortho*, *meta* and *para* substituted anilines, however, can be achieved using the triazeno moiety as a protecting

group via a modified Sandmeyer reaction.⁵⁷ In regards to the use of triazenes as *in situ* diazonium ions sources, aromatic fluorination and nanotubes functionalization in aqueous solutions represent two of the most important applications.⁵⁸⁻⁶⁰

Triazenes also play a relevant role in clinical investigations because of their antitumor activity.^{61,62} Structural requirements of triazene antitumor agents are depicted in Figure 1-4.⁶² The substituent on N¹ has little effect on the antitumor activity and can simply be taken as a carrying group, while the substituents on N³ matter a lot (*i.e.*, there should be a methyl group and a good leaving group that can be readily lost in a metabolic process).^{62,63}

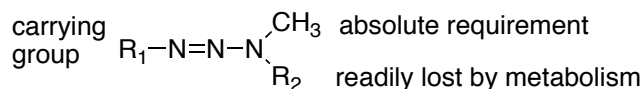
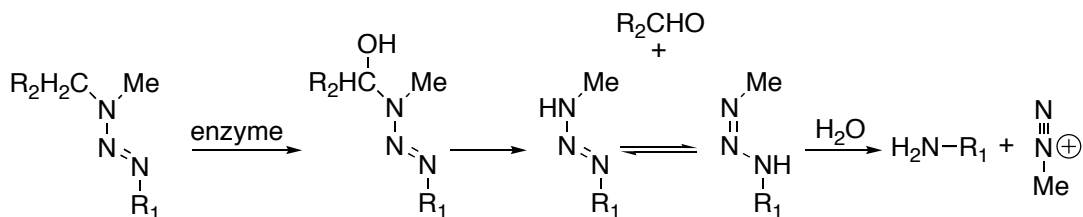


Figure 1-4. Structural requirements of triazene antitumor agents

A commonly accepted metabolism mechanism is illustrated in Scheme 1-14.⁶³ The initial enzyme catalyzed dealkylation is followed by rearrangement of the resulting disubstituted triazene and proteolytic loss of an amine to generate the methyldiazonium ion, a highly reactive species that methylates the target tumor molecules.⁶³



Scheme 1-14. Metabolism of antitumor triazenes

The fact that methyldiazonium ions can also react with DNA purinic bases, forming methyl adducts, makes triazenes carcinogenic or mutagenic.⁶¹ The cytotoxic and mutagenic effects of triazenes depend on the efficiency of DNA repair mechanisms; detailed information about triazenes antitumor activity and related DNA repair systems can be found in a review written by Marchesi et al.⁶³

1.2. Cyclodextrins

Cyclodextrins (CDs), also known as cycloamyloses and Schardinger dextrins, are oligomers of α -glucose obtained by the action of enzymes on starch.⁶⁴ CDs are designated by a Greek letter to denote the number of glucose units: α - for six, β - for seven (Figure 1-5), and γ - for eight. The most abundant α -, β - and γ -CDs are commonly referred to as native CDs, among which β -CD is the most popular and readily accessible one.

The glucose units in CDs are connected by α -(1,4) bonds, as shown in Figure 1-5 (left) for β -CD.⁶⁴ The consequence of this bonding mode is the formation of a donut-shaped structure (Figure 1-5, right), with one broader rim lined with $2 \times n$ secondary hydroxyl groups, the other narrower rim lined with n primary hydroxyl groups, and the interior of the cavity lined with a row of C3-H groups, then a row of ether-like glycosidic oxygens, and then a row of C5-H groups.⁶⁴

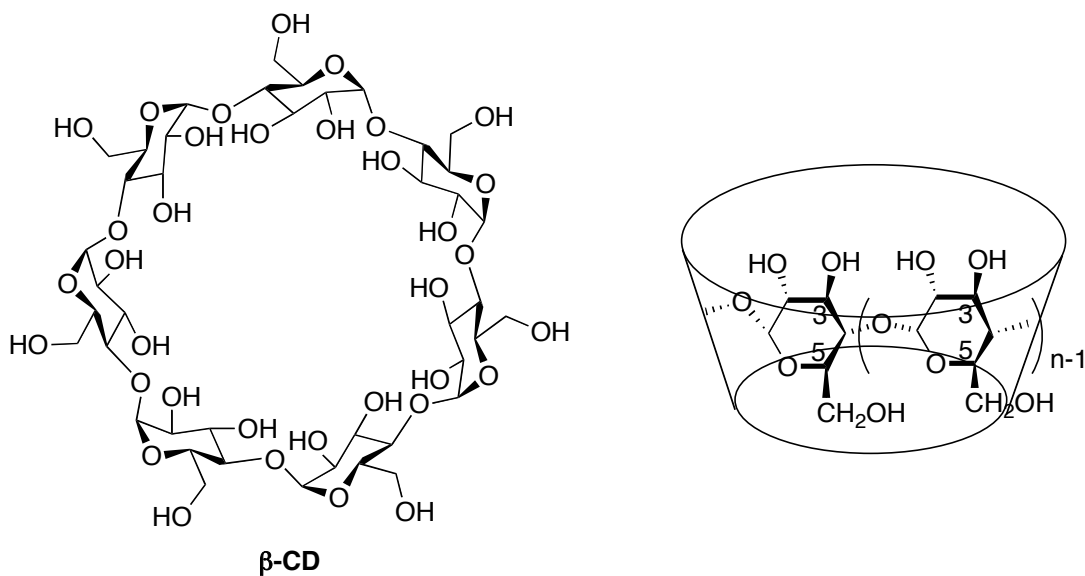


Figure 1-5. Cyclodextrins structure

The CD hydroxyl groups are nucleophilic in nature, and a series of modifications can be achieved by electrophilic attack on these positions.^{64,65} Among the three kinds of hydroxyl groups, primary C6-OH groups are the most basic and nucleophilic ones, C2-OH groups are the most acidic while C3-OH groups are the most inaccessible.⁶⁴ Thus, electrophilic reagents will initially attack C6-OH groups; more reactive reagents can further react with C2-OH and C3-OH groups. The electrophilic attack does not simply depend on the position of the hydroxyl groups of CDs; the size of the CD cavity also has an effect on the reaction site. For example, in alkaline aqueous solutions, tosyl chloride reacts with α -CD to give C2-tosyl- α -CD, while with β -CD, it gives C6-tosyl- β -CD.⁶⁶

The above mentioned structural characteristics make CDs to have fairly polar hydrophilic exteriors and relatively non-polar hydrophobic interiors, which result in two of the most important properties of CDs: (1) aqueous solubility and (2) lipophilic molecules encapsulation. Some basic physical properties of native CDs at room

temperature (25°C) are listed in Table 1-1.⁶⁷ The inner diameter of the cavity of the native CDs varies from 5 Å to 8 Å, and the cavity is about 7.9 Å in depth.⁶⁷ Thus, the cavity of α -CDs is suitable for encapsulating molecules with the size of a benzene ring or low molecular weight compounds with aliphatic side chains; β -CDs complex aromatics and heterocycles; and γ -CDs can accommodate larger guests such as macrocycles and steroids.⁶⁸

Table 1-1. Physical properties of native CDs^{67,69}

CD	Molecular weight	pK _a	Water solubility (g/100mL)	Internal Diameter (Å)	Number of water molecules inside the cavity
α -CD	972.85	12.33	14.5	4.7-5.2	6
β -CD	1134.99	12.20	1.85	6.0-6.4	11
γ -CD	1297.14	12.08	23.2	7.5-8.3	17

1.2.1 Inclusion complexes

There are two critical factors that determine the formation of inclusion complexes between cyclodextrins and guest molecules. The first one is the relative size of the cyclodextrin cavity to the size of the guest molecule or of certain key functional group(s) within the guest. If the guest is not of the appropriate size, it will not fit properly into the cyclodextrin cavity. The second factor encompasses the thermodynamical interactions between the different components of the system (CDs, guests, and solvents). There must be a favorable net energetic driving force that pulls the guest into the cyclodextrin cavity.⁶⁸

CD inclusion complexes are mainly formed via substitution of included water molecules by appropriate guest species; release of high-energy water molecules decreases the energy of the system.⁷⁰ There is no covalent bonding between guests and hosts; other factors such as van der Waals interactions, hydrogen bonding, hydrophobic interactions, release of strain energy in the macromolecular ring of the cyclodextrins and changes in solvent-surface tensions contribute to the formation of CD inclusion complexes as well.⁷¹

Cyclodextrins have been widely applied in pharmaceutical industry, especially in drug formulations, to enhance the solubility, stability, and bioactivity of drug molecules through the formation of inclusion complexes.^{64,65} Usually a 1:1 guest:host interaction is seen but other order complexes (such as 1:2, 2:2, or 2:1) have been seen as well. Since native CDs have relatively low solubility in both aqueous and organic solutions, their uses in pharmaceutical formulations are limited.⁶⁴ Thousands of modified CDs have been synthesized in order to achieve better properties (*e.g.*, better solubility, better complexation stability and less toxicity) than those of native CDs.⁶⁵ Three main types of derivatives have been developed: hydrophilic (methylated, hydroxyalkylated, and branched), hydrophobic (ethylated), and ionic (sulphated and phosphated). Table 1-2 lists some examples of modified CDs with improved solubility.⁷² In addition, CDs have been reported to enable mixing of incompatible drugs, prevention of drug-drug interactions, reduction of unpleasant drug tastes, protection from ultraviolet irradiation, oxidation, and hydrolysis of drugs, provision of a constrained medium for chemical synthesis, emulsification of hydrocarbons, steroids, and fats, conversion of liquid materials to dry form, and fixation of volatile compounds.⁷³

Table 1-2. Physical properties of some CD derivatives (25°C)⁷²

CD	O-substituent	Substitution degree ^a	Molecular Weight	Water solubility (g/100ml)
2-HP-β-CD ^b	-CH ₂ CHOHCH ₃	0.65	1400	> 60
RM-β-CD ^c	-CH ₃	1.8	1312	> 50
2-HP-γ-CD ^d	-CH ₂ CHOHCH ₃	0.6	1576	> 50

^a Average number of substituents per glucose unit. ^b 2-Hydroxypropyl-β-CD. ^c Randomly methylated-β-CD. ^d 2-Hydroxypropyl-γ-CD.

The ability to form inclusion complexes with a variety of guest molecules makes CDs of utility not only for pharmaceutical use, but also in cosmetics (*e.g.*, sunscreen creams, toiletry), foods and flavors, agriculture and environmental science. CDs are used in the preparation of sunscreen lotion as the CD cavity limits the interaction between the UV filter and the skin, thus reducing the side effects of the formulation.⁶⁸ By forming inclusion complexes, the release of fragrances can be controlled, thus making the fragrance long lasting.⁶⁸ Most natural and artificial flavors are volatile oils or liquids and complexation with CDs provides a promising alternative to the conventional encapsulation technologies used for flavor protection.⁶⁸ CDs are also used as process aids in food; for example, β-CD can be used to remove cholesterol from milk and produce dairy products low in cholesterol; α-CD can stabilize emulsions like mayonnaise, margarine and butter creams.⁷⁴ In agriculture, CDs can be applied to delay germination of seed. In grain treated with β-CD, some of the amylases that degrade the starch supplies of the seeds are inhibited. Initially the plants grow more slowly, but later on, this is largely compensated by a larger harvest improvement.⁷⁴ CDs play a major role in environmental

science in terms of solubilization of organic contaminants, enrichment and removal of organic pollutants and heavy metals from soil, water and the atmosphere.⁷⁵

CDs have been widely used in different separation technologies as well; CDs can be used as chemically bonded or sorbed ligands in stationary phase or as solution additives.⁷⁵ The shape and size selectivity of CDs provide the bases for compounds separation, because the binding constants of various molecules with CDs are of different magnitude, thus, molecular discrimination can be achieved. Table 1-3 shows binding constants (K_B) for different organic molecules with native CDs.⁷⁵ In addition to the size, the electron density of the guest molecule affects the strength of the complexation too. The non-bonding electron pairs of the glycosidic oxygen bridges are directed toward the inside of the cavity thus making an electron rich environment in the cavity;⁶⁷ thus, nonionized species generally bind more strongly to the native CDs than their charged equivalents (Table 1-4).⁷⁵

Table 1-3. Dependence of binding constants on solute and cyclodextrin cavity size.⁷⁵

Guest	K_B (M^{-1})		
	α -CD	β -CD	γ -CD
1,3-Butanediol	16200	12023	
4-Methoxy-cinnamic acid	10300	658	
Adamantane carboxylic acid	130	330000	24000
Testosterone	5058	7540	16500
Naphthalene	77	608	130
Anthracene	40	2300	1500
Phenanthrene	60	1500	770

Table 1-4. Binding constants for neutral and ionized forms of various solutes and β -CD.⁷⁵

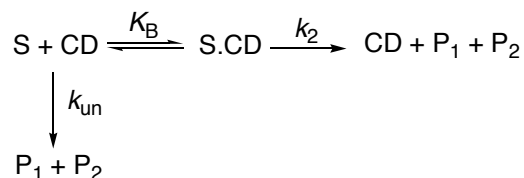
Guest	K_B (M^{-1})	
	<i>neutral</i>	<i>anion</i>
Barbital	210	100
Benzoic acid	632	35
n-Decanoic acid	9440	6730
Hexobarbital	1280	380
	<i>neutral</i>	<i>cation</i>
Aminoadamantane	110000	8430
4-Nitroaniline	300	100
Morpholine	17	7

1.2.2 Catalysis

CDs can catalyze reactions through inclusion complex formation.⁶⁴ Catalysis by CDs can be divided into two categories: (a) covalent catalysis (in which a covalent intermediate is formed between the CD and the substrate, which subsequently renders the product) and (b) non-covalent catalysis (in which CDs participate in the reactions in a non-covalent manner).^{64,70a}

The first step in covalent catalysis involves inclusion complex (S.CD) formation between the CD and the substrate (S); subsequently, the CD hydroxyl groups react with the substrate and form a covalent intermediate CD_P₁, which gives rise to the final products (P₁ and P₂) while CD is regenerated (Scheme 1-15). CDs provide their cavities as chemically and sterically specific reaction fields, making the chemical transformation

resulting in acceleration (or deceleration) of reactions.^{64,70b} The general mechanism for non-covalent catalysis can be illustrated as shown in Scheme 1-16.



Scheme 1-16. Non-covalent catalysis by CDs

Non-covalent catalysis by CDs can be attributed to two effects: a) conformational effects (since the cavity of CDs is spatially restricted) and b) microsolvent effects (which arise from the apolar character of the CD cavity).^{70b} When guest molecules accommodate into the CD cavity, they take specific orientations due to the above two effects, thus only selective reactions can occur. Furthermore, it is not uncommon to find that only one conformational isomer can be encapsulated in the cavity or that is more favorable to be encapsulated than other isomers. Thus, CDs exhibit catalysis or inhibition of reactions depending on what guests and how the guests are encapsulated in the CD cavity;^{64,70b} Table 1-5 lists some examples of reactions that are catalyzed or inhibited by CDs.

Table 1-5. Examples of reactions catalyzed or inhibited by CDs

CD	Guest	Reaction	k_{CD}/k_{un} ^a	Ref.
COP- β -CD ^b	2-Hydroxybenzyl alcohol	Oxidation	6.3×10^4	79
PFD- α -CD ^c	2-Hydroxyaniline	Oxidation	410	80
β -CD	<i>o</i> -Methyl red	<i>Cis-trans</i> isomerization	0	81
DM- β -CD ^d	4-Methoxybenzoyl chloride	Hydrolysis	2.15×10^{-3}	82

^a k_{CD} represents the reaction rate constant for complexed substrate, while k_{un} represents the reaction rate constant for free substrate. ^b 6^A,6^D-Di-C-oxo-6^A,6^D-O-(2-oxo-1,3-propanediyl)- β -CD. ^c 6^A,6^D-Di-O-(2-formyl-1,3-propanediyl)- α -CD ^d Heptakis(2,6-di-O-methyl)- β -CD.

1.3 Research objectives

As already stated, triazenes are well known photochromic materials due to their ability to undergo reversible photoinduced *cis-trans* isomerization around the N=N double bond. In addition, their nucleophilic character gives rise to their frequent application in spectrophotometric methods for detection and quantitative determination of metal cations upon complexation. One of the objectives of the work presented in this thesis is to probe the effects of metal cations on the photochromic reactivity of triazenes. Interest for this type of study arises from the potential application of triazenes and metal cations in photoswitchable sensing devices, which can enable monitoring metal ions by color change upon complexation, and forcibly releasing absorbed ions upon *cis-trans* isomerization.

As mentioned in Section 1.1.3.2, the acid-induced heterolytic cleavage of triazenes N2-N3 bond constitutes the basis of many applications in synthetic and biological areas.

Cyclodextrins, macrocycles that can alter guest molecules properties through inclusion complexes formation, have been widely used in pharmaceutical applications. The other objective of the work presented in this thesis is to study the effects of CDs on the rate of acid-catalyzed 1,3-diphenyltriazenes decomposition. Interest for this type of study arises from the potential capability of CDs to control the rate of decomposition and hence, control the rate of *in situ* production of anilines and diazonium ions, which are widely used in organic synthesis.

Chapter 2. Metal-triazene complexes

To probe the effects of metal cations on the photochromic properties of triazenes, three 1,3-diphenyltriazenes (Chart 2-1), the parent 1,3-diphenyltriazene (HDPT) and two other derivatives with either an electron-donating group (4-CH₃O) or an electron-withdrawing group (3-CF₃), were selected as target substrates. The metal cations chosen for the project were Ag⁺ (AgNO₃) and Hg²⁺ (HgCl₂). As mentioned in Section 1.1.2, Ag⁺ is a representative monovalent metal cation, able to form complexes with different triazenes. Hg²⁺ was chosen as a representative bivalent cation, since other candidates like Zn²⁺, Cu²⁺ and Fe²⁺ may catalyze substrate decomposition.⁸³ In addition, both Ag⁺ and Hg²⁺ have filled *d* orbitals (4*d*¹⁰ for Ag⁺, 5*d*¹⁰ for Hg²⁺) so they do not absorb in the near UV and visible regions⁸⁴ and, therefore, will not absorb photons at 355 nm, which is the excitation wavelength used to induced *trans*-to-*cis* photoisomerization of target triazenes.

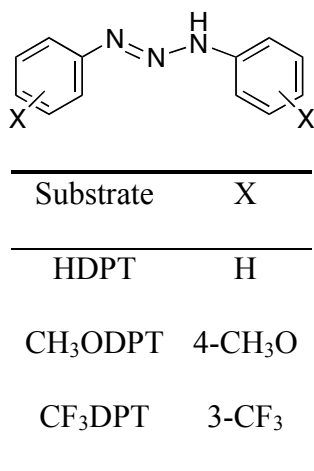


Chart 2-1. Structure and abbreviation of target substrates

Experiments were carried out in aqueous solutions at pHs high enough to diminish substrate decomposition, since triazenes are sensitive to the presence of acids (see Section 1.1.1.2). Two photometric techniques were applied in this study: UV-visible absorption spectroscopy (used to monitor the formation of metal cation-triazene complexes as well as to determine the stoichiometry of the complexes) and laser flash photolysis (LFP, used to monitor the thermal *cis-to-trans* isomerization process).

2.1 Results

2.1.1 UV-visible absorption spectroscopy

Complexation of triazenes with metal cations was monitored by recording absorption spectra of solutions containing a constant concentration of the triazene and increasing concentrations of the metal cation. The spectra obtained in this manner are often referred to as absorption titration spectra.⁸⁵ The method of continuous variation (also known as Job's method) was used to determine the stoichiometry of the predominant complex.⁸⁵ In this method, the total concentration of triazene plus metal cation is kept constant, while the [metal cation]/[substrate] ratio is varied. A graph is made by plotting the corrected absorbance (*i.e.*, $\Delta A_c = \text{measured absorbance} - (\text{metal cation absorbance} + \text{substrate absorbance})$) as a function of the metal ion molar fraction. A maximum absorbance is reached at the stoichiometric molar ratio of the predominant complex.⁸⁵ The plot approaches two straight-line segments when the binding constant of the complex is very large, and the apex of the angle yields the stoichiometry of the complex.⁸⁶ Deviations of the plot from the theoretical straight lines can be used to estimate the binding constant of the complex.⁸⁷

2.1.1.1 HDPT

Experiments with HDPT as ligand and AgNO_3 or HgCl_2 as metal cation source were carried out at pH 9 and 13, in 2% MeOH (v/v) aqueous buffer solutions. Figures 2-1 and 2-2 show absorption titration spectra corresponding to Ag^+ and Hg^{2+} , respectively.

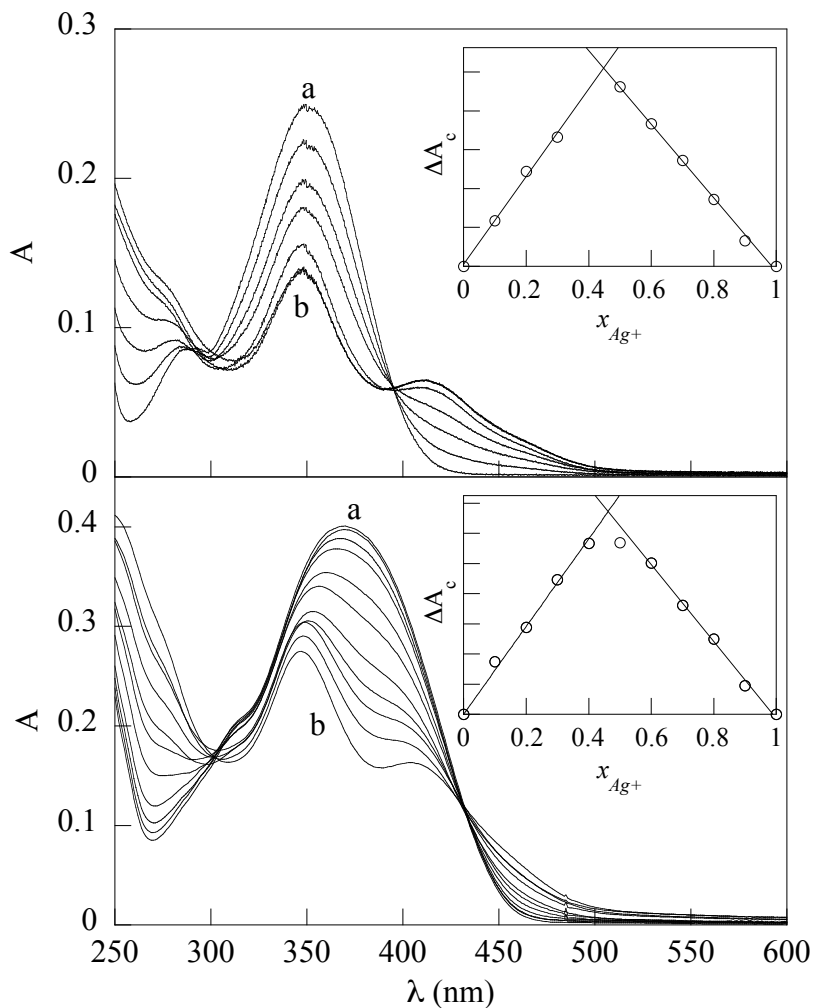


Figure 2-1. Absorption titration spectra of HDPT with Ag^+ in 2% MeOH aqueous solution; top: pH 9, $[\text{HDPT}] = 1.35 \times 10^{-5} \text{ M}$, $[\text{Ag}^+] = 0$ to $1.35 \times 10^{-5} \text{ M}$ (from a to b); bottom: pH 13, $[\text{HDPT}] = 2.62 \times 10^{-5} \text{ M}$, $[\text{Ag}^+] = 0$ to $2.35 \times 10^{-5} \text{ M}$ (from a to b). Inset: corresponding Job's plot.

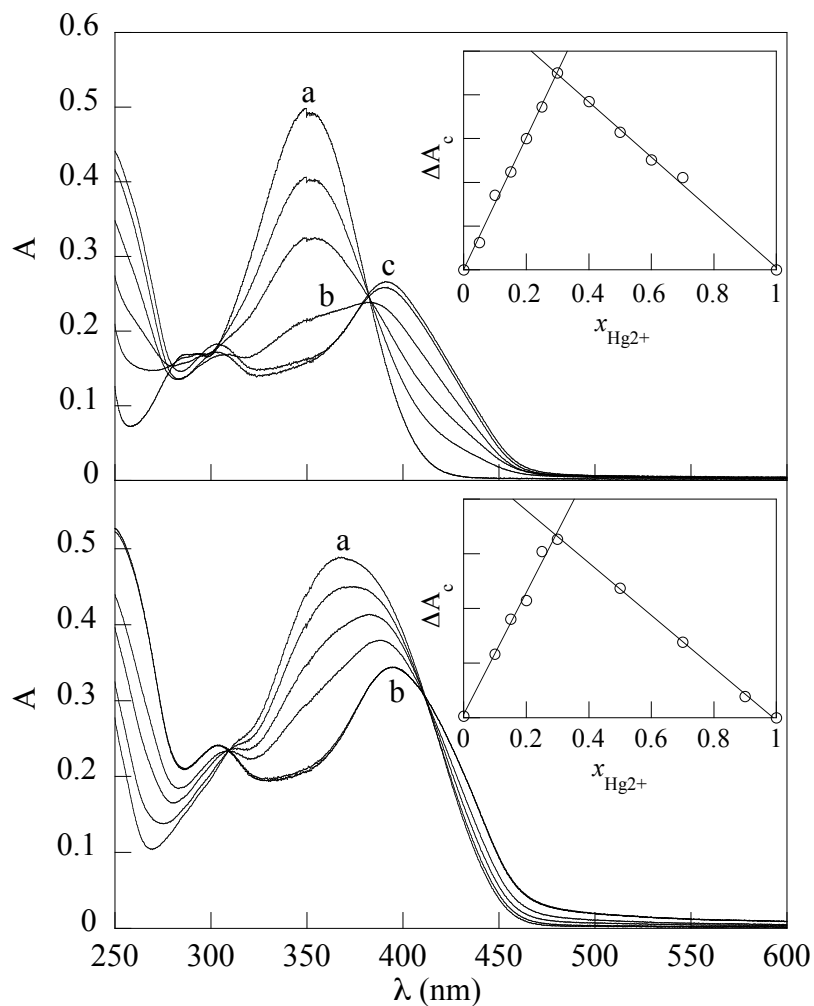


Figure 2-2. Absorption titration spectra of HDPT (3.08×10^{-5} M) with Hg^{2+} in 2% MeOH aqueous solution; top: pH 9, $[\text{Hg}^{2+}] = 0$ to 1.26×10^{-5} M (from a to b to c); bottom: pH 13, $[\text{Hg}^{2+}] = 0$ to 1.67×10^{-5} M (from a to b). Inset: corresponding Job's plot.

In all cases, the intensity of the absorption band centered at around 350 nm, which arises from the π - π^* transition associated with the N=N double bond,^{88,89} decreases with increasing metal cation concentration and a new absorption band at longer wavelength appears (~ 412 nm for Ag^+ , ~ 394 nm for Hg^{2+}). These spectral changes are good evidence

of complex formation between HDPT and Ag^+ or Hg^{2+} , and are consistent with the observation that upon metal cation addition the solutions turn yellow. Comparison of the absorption spectra for HDPT in aqueous solutions at pH 9 and pH 13 shows that at pH 13, the most intense peak, which arises from the π - π^* transition associated with the N=N double bond, is much broader than that at pH 9 and the wavelength of maximum absorption (λ_{max}) shifts to the red. Since the pKa for HDPT in 2% MeOH aqueous solution is *ca.* 13,⁹⁰ at this pH the neutral form and the anionic form of the substrate exist in *ca.* 1:1 ratio. Thus, the spectrum of the solution is the sum of the spectra for two absorbing species, *i.e.*, neutral and anionic triazene. The charge of the anionic form of triazene is further delocalized by conjugation. The effect of charge delocalization by conjugation is to lower the π^* energy level and give it less anti-bonding character; as a result, the absorption maximum is shifted to a longer wavelength.⁹¹ Thus, since the anionic form of triazene absorbs at a longer wavelength in comparison to the neutral form, the spectrum of the sum of neutral and anionic forms becomes broader and λ_{max} shifts to the red, relative to the spectrum of the neutral form. This also explains why at pH 9 solutions of HPDT were colorless while at pH 13 the solutions were light yellow.

In the spectra shown in Figures 2-1 and 2-2 there is at least one isosbestic point, which indicates that there are two stoichiometric states in a chemical equilibrium.⁹² Thus, it can be concluded that in each set of reactions corresponding to each of the spectra above, the two absorbing species in equilibrium are the free triazenes and the complexed ones.

The stoichiometry of the silver and mercury complexes was determined using the continuous variation method (Job's method). Theoretically, a Job's plot for a 1:1 complex yields a maximum at a molar fraction at 0.5, whereas that of a 1:2 complex yields a

maximum at 0.33. The insets of Figures 2-1 and 2-2 show, respectively, sharp maxima at mole fractions of 0.45 (top plot) and 0.47 (bottom plot) for silver complexes, and 0.30 (both plots) for mercury complex. The sharp shape of the Job's plots reveals large binding constants for both silver and mercury complexes. The values of the metal molar fractions corresponding to the maximum corrected absorbance reveals that, within experimental error, the stoichiometry (metal:ligand) for the silver complex is 1:1 while that of the mercury complex is 1:2 in aqueous solutions. These stoichiometric ratios are the same as those reported for solid state complexes, in which the amino H of 1,3-disubstituted triazines has been substituted by Ag^+ or Hg^{2+} cation.⁹³ Hence, one would expect that, if the amino H is also replaced by the metal cation in aqueous solutions, the absorption spectra of the complexes should not change with pH. Spectra for solutions containing HPDT and Ag^+ or Hg^{2+} (in 1:1 and 2:1 ratios, respectively) were recorded at pH 9, 10, 13 and 14, in 2% MeOH (v/v) aqueous solutions. As already mentioned, the pK_a of HDPT is *ca.* 13, thus, at pH 9 and 10, the substrate exists mainly in its neutral form, while at pH 14, the substrate exists mainly in its anionic form. It turns out that for both silver and mercury complexes, the shape of the spectra is pH independent, in agreement with the assumption that the amino H is substituted by the metal ion. However, it should be pointed out here that a slight variation (if at all significant) in absorbance with increasing pH is observed (typically, the higher the pH, the higher the absorbance), and that for both silver and mercury the solubility of the complexes is higher at pH 13 than in pH 9 solutions.

Experiments with higher organic co-solvent concentrations (30% MeOH and 30% THF) and in pure organic solvents (MeOH and MeCN) were also carried out. Spectra of

solutions with a stoichiometric ratio of metal:triazene in 30% MeOH and 30% THF aqueous solutions resemble the spectra previously recorded in 2% MeOH aqueous solutions. This may be an indication of co-solvent insensitivity of the absorption spectra of the metal complexes in aqueous solutions. On the contrary, in organic solutions, even with a large excess amount of metal cations, the spectra resemble the spectrum of HDPT itself, only slight spectral changes are observed, but are relatively more obvious in MeOH than in MeCN.

2.1.1.2 CH₃ODPT

Experiments with CH₃ODPT were carried out in 2% MeOH (v/v) and 30% MeOH (v/v) aqueous solutions, at pH 9 and 13. Figure 2-3 shows spectra of CH₃ODPT in the absence and in the presence of Ag⁺ (1:1 ligand:metal) or Hg²⁺ (2:1 ligand:metal) in 2% MeOH aqueous solution at pH 13. As in the case of HDPT, spectral changes indicate the formation of complexes, and the pH independent spectra of the complexes indicate the replacement of the amino H. Unfortunately, due to the substrate instability in aqueous solutions, neither the titration absorption spectra nor the Job's method plot could be obtained.

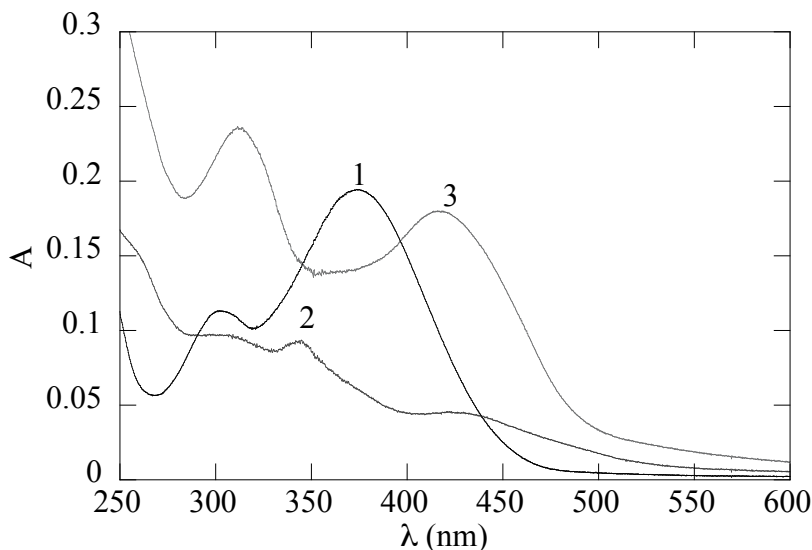


Figure 2-3. Absorption spectra of CH_3ODPT (1.26×10^{-5} M) in the absence (**1**) and presence of metal cations (**2**, $[\text{Ag}^+] = 1.26 \times 10^{-5}$ M; **3**, $[\text{Hg}^{2+}] = 0.63 \times 10^{-5}$ M) in 2% MeOH aqueous solutions at pH 13.

2.2.1.3 CF_3DPT

Experiments with CF_3DPT as ligand and Ag^+ or Hg^{2+} were carried out in 30% (v/v) MeOH and 30% THF (v/v) aqueous solutions, at pH 9 and 13. Due to the limited solubility of the complexes in 30% MeOH aqueous solutions (precipitate comes out when metal cation is added to the substrate at a concentration of $\sim 1.4 \times 10^{-5}$ M), absorption titration spectra and the stoichiometry of the complexes were determined using 30% THF (v/v) aqueous solutions.

Figure 2-4 shows the spectra of the substrate (a) and of the silver-triazenide complex (b). The Job's plot (Figure 2-4 inset) with a joint point at 0.45 reveals that for CF_3DPT , silver cation forms a 1:1 complex, as in the case of HDPT. The same spectral changes upon complexation as with the previous two substrates are seen here, *i.e.*, the intensity of

the main peak decreases while a new absorption band appears at a longer wavelength. Experiments at pHs higher than 13 were not feasible, because Ag^+ was not stable in alkaline 30% THF aqueous media. The solutions became darker and darker as time passed by, which may be attributed to formation of the dark brown Ag_2O in hydroxide solutions.⁹⁴

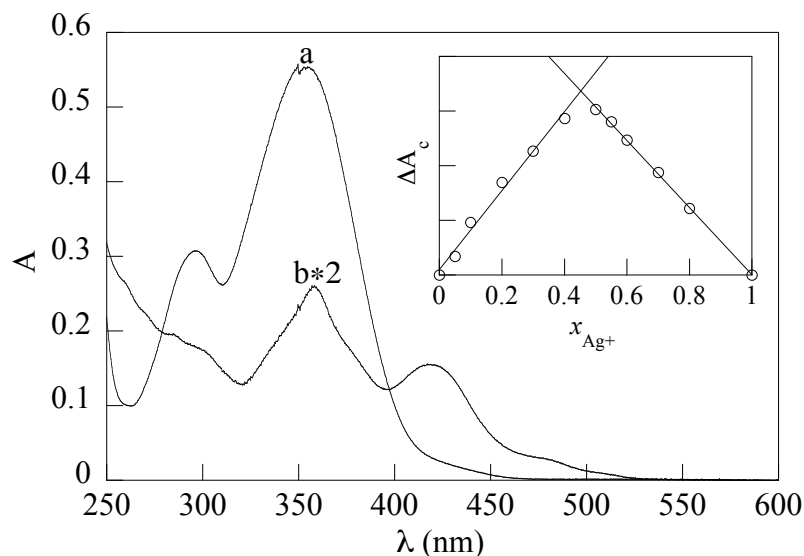


Figure 2-4. Absorption spectra of CF_3DPT and of its silver complex in 30% THF aqueous solution at pH 9: (a) $[\text{CF}_3\text{DPT}] = 2.82 \times 10^{-5} \text{ M}$; (b) $[\text{CF}_3\text{DPT}] = [\text{Ag}^+] = 1.41 \times 10^{-5} \text{ M}$. Inset: corresponding Job's plot.

The absorption titration spectra and Job's plot for Hg^{2+} in 30% THF aqueous solutions at pH 9 and 13 are shown in Figure 2-5. The spectral changes upon metal cation addition, *i.e.*, decrease in intensity of the main peak and appearance of a new peak at a longer wavelength, indicate metal complex formation. The observation that the shape of the absorption spectrum of the complex remains unchanged at different pHs once again

reveals that it is the triazenide which forms the complex. There is at least one isosbestic point in each set of spectra, which again indicates free triazene and complexed triazene at equilibrium. The joint point at 0.31 and 0.27 in the Job's plots indicate that Hg^{2+} forms a 1:2 (metal:ligand) complex with CF_3DPT in aqueous solutions.

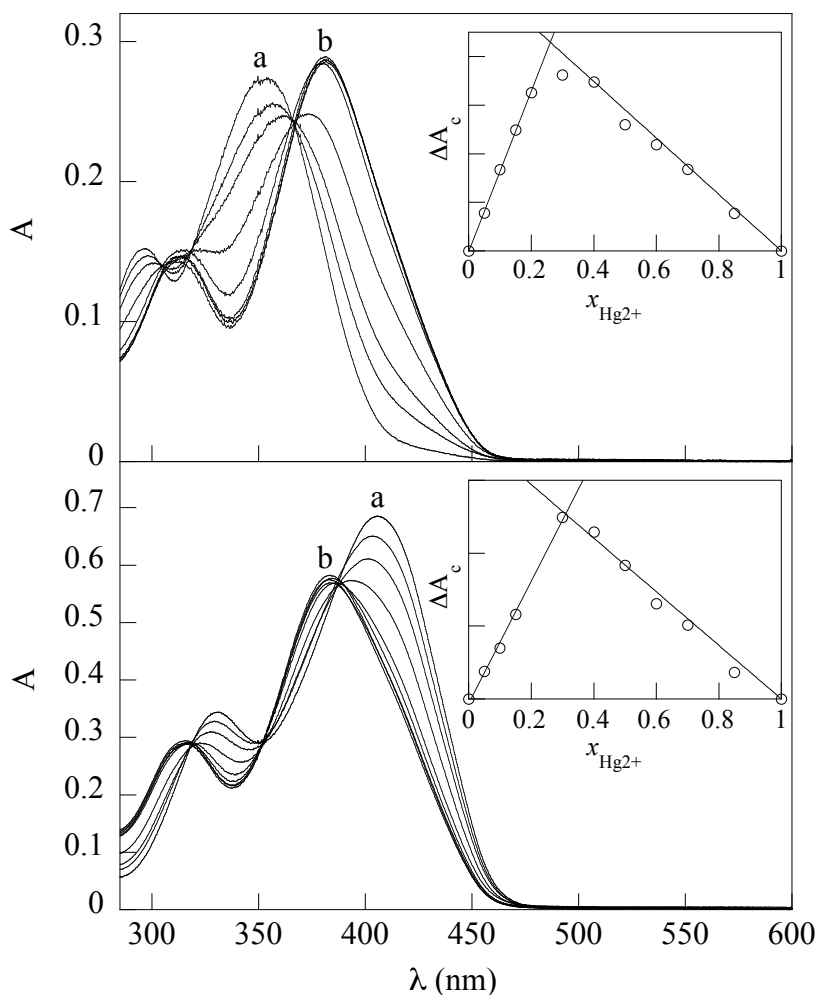


Figure 2-5. Absorption titration spectra of CF_3DPT with Hg^{2+} in 30% THF aqueous solutions; top: pH 9, $[\text{CF}_3\text{DPT}] = 1.41 \times 10^{-5} \text{ M}$, $[\text{Hg}^{2+}] = 0$ to $2.82 \times 10^{-5} \text{ M}$ (from a to b); bottom: pH 13, $[\text{CF}_3\text{DPT}] = 2.68 \times 10^{-5} \text{ M}$, $[\text{Hg}^{2+}] = 0$ to $3.22 \times 10^{-5} \text{ M}$ (from a to b). Inset: Job's plot.

2.1.2. Laser flash photolysis (LFP)

Trans-cis isomerization of triazenes in aqueous solutions can be monitored using a LFP system. *Cis*-triazenes are obtained by laser excitation at 355 nm of *trans*-triazenes, and the *cis*-to-*trans* isomerization is a spontaneous thermal process. Transient absorption spectra for triazenes reveal that at $\lambda > 350$ nm, *cis*-triazenes have lower absorptivity than their corresponding *trans*-forms.¹⁰ Thus, the LFP signal, which is a measurement of the absorption difference between the absorption of the solution before and after laser excitation, will be negative.⁹⁵ Kinetic traces for laser induced isomerization of triazenes show an instantaneous bleaching (due to *trans*-to-*cis* photoisomerization), followed by a complete recovery of the signal (resulting from thermal *cis*-to-*trans* isomerization), as illustrated in Figure 2-6 for isomerization of HDPT in 2% MeOH aqueous solution at pH 13.

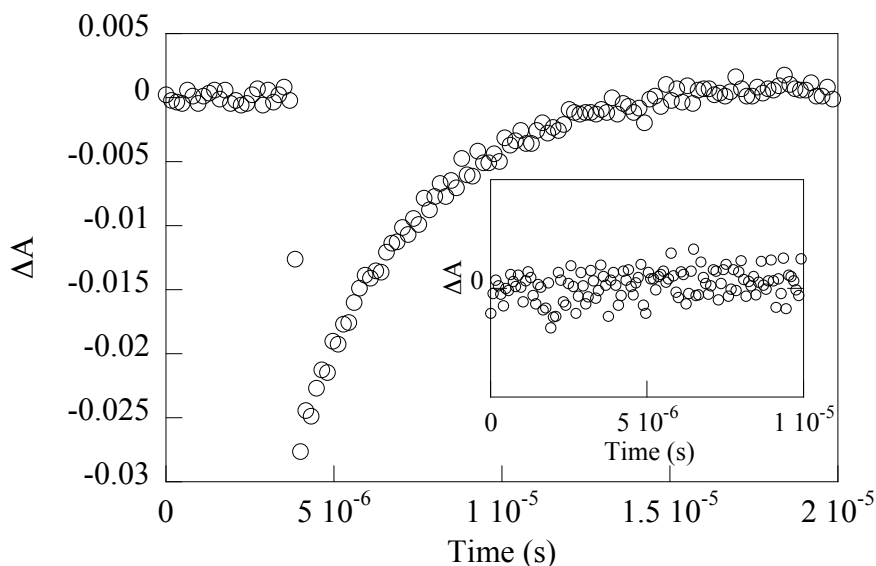


Figure 2-6. Laser induced kinetic trace for HDPT (2.62×10^{-5} M) in 2% MeOH aqueous solution at pH 13. Inset: laser induced kinetic trace for HDPT (2.62×10^{-5} M) in the presence of an equimolar amount of Ag^+ in 2% MeOH aqueous solution at pH 9.

Unfortunately, regardless of the pH and substrate, upon addition of stoichiometric amounts of metal cations, no LFP signals could be observed (a typical trace is shown in Figure 2-6 inset), indicating that target metal-*trans*-triazenide complexes do not photoisomerize.

2.2 Discussion

Upon complexation with metal cations, the longest wavelength absorption band appears to the right in comparison to that of free triazene, and a decrease in absorption where the free triazene absorbs is observed. Table 2-1 lists the absorption bands of the three substrates employed in this study and of their corresponding silver and mercury complexes.

Table 2-1. Absorption bands of triazenes and of their metal complexes in aqueous solutions.^a

	HDPT	CH ₃ ODPT	CF ₃ DPT
None	285 (295); 350 (360)	300 (302); 373 (370)	296; 352
Ag ⁺	348; 412	345; 425	358; 417
Hg ²⁺	303 (305); 394 (390)	312 (310); 415(400)	312; 382

^aData in parenthesis are from Ref. 96 for benzene as solvent.

Table 2-1 indicates that, in aqueous solutions, the silver-triazenide complexes have two peaks at around 350 nm and 415 nm, while mercury-triazenide complexes have two peaks at around 310 nm and 390 nm. In addition, the spectra of HDPT and CH₃ODPT as

well as of their corresponding mercury complexes obtained in aqueous solutions are similar to the spectra reported for benzene as solvent.⁹⁶ This might be an indication that, for these systems, the dipole moment of the electronic ground state is similar to that of the excited state, since a pronounced solvatochromism should be observed if the charge distribution and consequently the dipole moment in the electronic ground state is considerably different from that in the excited state.⁹⁷ In fact, absorption spectra of HDPT and CH₃ODPT recorded in 2% MeOH aqueous solution, MeOH and THF, display only a small bathochromic λ_{max} shift with decreasing polarity ($\Delta\lambda_{\text{max}} = 4$ nm for HDPT, 3 nm for CH₃ODPT).

As indicated in the previous section, the sharp shape of the Job's plots is a good indication of large binding constants for the complexes involved in this study. In all cases, it is observed that complexation occurs as rapidly as the two reactants can be put together, indicating that a fast equilibrium takes place between the triazene and metal cation. Experiments to test if the metal cations are exchangeable were also carried out. Excess amount of Ag⁺ was added to solutions containing stoichiometric amounts of Hg²⁺ and HDPT, and excess amount of Hg²⁺ was added to solutions containing stoichiometric amounts of Ag⁺ and HDPT. In no case did addition of a second metal cation species change the spectrum of the solution; in other words, once the complex is formed, it is very stable and the metal cations are not exchangeable. This result is consistent with the fact that metal ions in the second and third transition series are generally kinetically inert.⁹⁸

Spectra of HDPT and metal cations in organic solvents resembling that of HDPT itself may be due to either the similarity between the spectra of the complexes and

corresponding triazene in organic solvents or the formation of the complex in very little extent, if any at all. The first possibility is very unlikely because it contradicts the above observation that the spectra characteristics of mercury-triazenide complexes in benzene and aqueous solutions are very similar while they are very different from the spectrum of HDPT. As mentioned in the results section, when the metal complexes are formed, metal cations take the place of the amino H; thus, the acidity of triazenes, which is a solvent dependent property, is expected to affect complex formation. Since H₂O is a stronger base than MeOH,^{97a} it would facilitate replacement of the amino H and hence, metal complex formation. Thus, one can assume that the binding constants of the metal complexes in organic solvents (*e.g.*, MeOH and MeCN) would be much smaller than those in aqueous solutions. This assumption is supported by reports on the synthesis of metal-triazenide complexes in organic solutions which indicate in the absence of triethylamine some of these reactions do not happen at all, or hours of stirring are needed.^{30,31,99,100} In addition, the fact that spectral changes are more obvious in MeOH than in MeCN would indicate that the complex can be formed, although to a very small extent, more easily in MeOH than in MeCN.

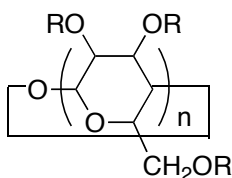
As mentioned in the results section, no isomerization of metal-triazenide complexes could be observed. Lack of photoisomerization of triazenide systems is not unprecedented; no laser signal could be detected upon photoexcitation of the anionic conjugate form of NO₂DPT (X = NO₂ in Chart 2-1).¹¹ Whether charge delocalization in the triazenide moiety, photoexcitation wavelength, and the chelating or bridging structure of the complexes play any role in preventing photoisomerization of metal-triazenide complexes are yet to be determined.

2.3 Conclusions

UV-visible absorption spectra show that target 1,3-diphenyltriazenes HDPT, CH₃ODPT and CF₃DPT can easily form complexes with Ag⁺ and Hg²⁺ cations in aqueous solutions. The stoichiometry (ligand:metal) of silver-triazenide complexes is 1:1, while that of mercury-triazenide complexes is 2:1. Unfortunately, metal complex formation prevents photoisomerization of the triazenide moiety, at least upon excitation at 355 nm.

Chapter 3. Cyclodextrin effects on triazenes decomposition

To investigate the effects of cyclodextrins on the acid-catalyzed decomposition of triazenes, two of the most water soluble 1,3-diphenyltriazenes, *i.e.*, HDPT and CH₃ODPT were chosen as substrates (guest molecules). Cyclodextrins varying in size, *i.e.*, α -CD, β -CD, and γ -CD, and with different rim substituents, *i.e.*, heptakis(2,3,6-tri-*O*-2-hydroxypropyl)- β -CD (HP- β -CD) and heptakis(2,3,6-tri-*O*-methyl)- β -CD (TM- β -CD), were employed as host molecules (Chart 3-1).

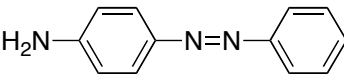


Host	n	R
α -CD	6	H
β -CD	7	H
γ -CD	8	H
HP- β -CD	7	CH ₂ CHOHCH ₃
TM- β -CD	7	CH ₃

Chart 3-1. Structure and abbreviation of host molecules

Kinetic measurements were carried out by means of UV-visible spectrometry, while a study on the binding of host and guest molecules was carried out using both UV-visible and circular dichroism spectrometric methods.

3.1 Results

Acid-induced decomposition of 1,3-diaryltriazenes can be easily followed by UV-visible spectroscopy, since they usually have strong absorptions around the 350 nm UV region, while their decomposition products do not. The time-resolved absorption spectra of HDPT at pH 6.16 (phosphate buffer) are shown in Figure 3-1. As for spectrum (a) in Figure 2-1 for HDPT at pH 9, the peak centered at 350 nm is ascribed to the π - π^* transition of the triazeno group;⁸⁸ since both pH 9 and 6 are far below the pK_a value of HDPT (*i.e.*, 13.0^{90b}) the spectra (a) at both pHs are of the neutral triazene. In Figure 3-1, the decrease in the intensity of the peak centered at 350 nm reflects the decomposition of HDPT. The peak at 263 nm, with an initial increase and subsequent decrease in intensity, is a good indication of a reaction intermediate (Figure 3-2), and is assigned to the diazonium ion. The assignment is based on the facts that (1) triazenes, as mentioned in Section 1.1.1.2, generate diazonium ions in acidic conditions, (2) the diazonium ion $C_6H_5N_2^+$ mainly absorbs at 260 nm in solutions,¹⁰¹ and (3) the formation of the intermediate has the same rate as the consumption of the triazene (Figure 3-2 inset). In addition, as the diazonium ion absorption band decreased in intensity, the absorbance at longer wavelengths (visible region) increased. This is ascribed to formation of a C-azo compound (), which also is a common byproduct in the synthesis of triazenes, through an electrophilic aromatic substitution reaction (C-coupling) between the diazonium ion intermediate and aniline.^{102,103}

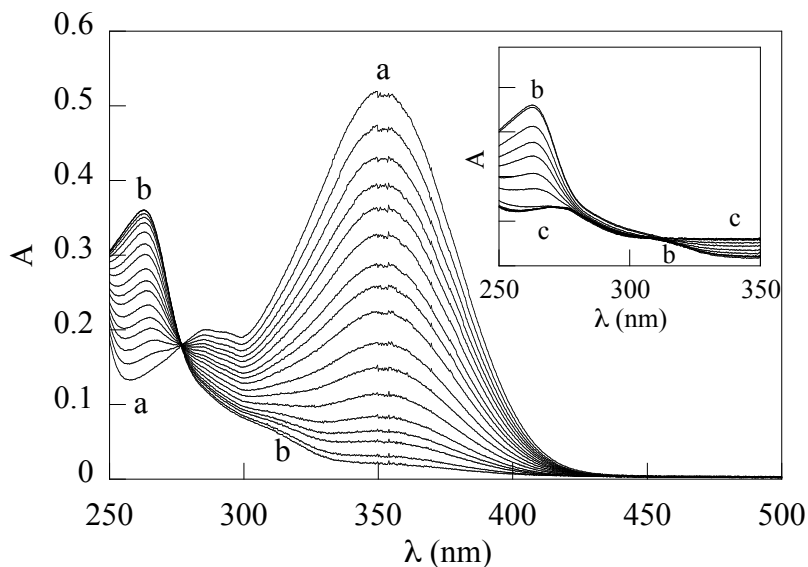


Figure 3-1. Time-resolved absorption spectra for decomposition of HDPT (3.2×10^{-5} M) in 2% MeOH aqueous solution at pH 6.16 (0.05 M phosphate buffer), obtained within 1 min and 45 min (from a to b) after sample preparation. Inset: corresponding spectra obtained within 45 min and 8 h (from b to c) after sample preparation.

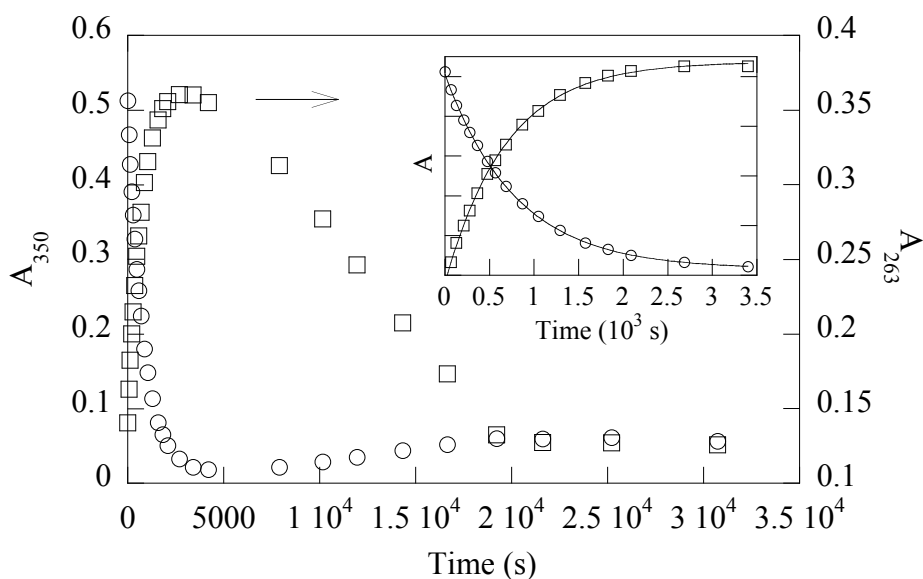


Figure 3-2. Absorption-time profile for decomposition of HDPT (3.2×10^{-5} M) in 2% MeOH aqueous solution at pH 6.16 (0.05 M phosphate buffer) monitored at 350 nm (○) and 263 nm (□). Inset: expanded profiles obtained within first 58 min.

Figure 3-3 shows the time-resolved absorption spectra of HDPT in the presence of 7 mM β -CD. When compared with Figure 3-1, the initial λ_{max} in Figure 3-3 shows a bathochromic (red) shift, while the maximum absorption wavelength corresponding to the diazonium ion intermediate remains at the same position (263 nm). The most significant observation in the presence of β -CD is that the decomposition of HDPT becomes much slower than in the absence of it (Figure 3-2 vs. 3-4). Formation of the C-azo compound still can be observed although to a smaller extent (Figure 3-3 inset), which may be ascribed to β -CD inhibition of the electrophilic aromatic substitution reaction as well.

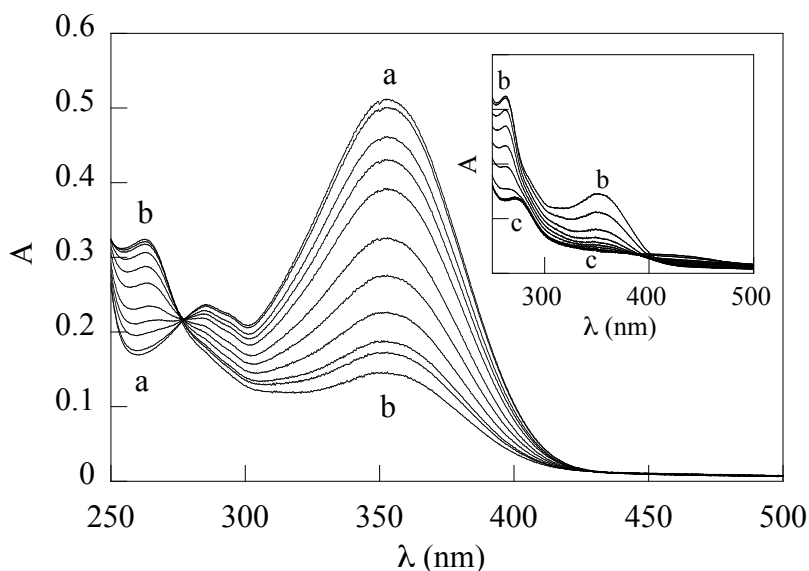


Figure 3-3. Time-resolved absorption spectra for decomposition of HDPT (3.2×10^{-5} M) in the presence of β -CD (7 mM) in 2% MeOH aqueous solution at pH 6.16 (0.05 M phosphate buffer), obtained within 1 min and 1.7 h (from a to b) after sample preparation. Inset: corresponding spectra obtained within 1.7 h and 8.0 h (from b to c) after sample preparation.

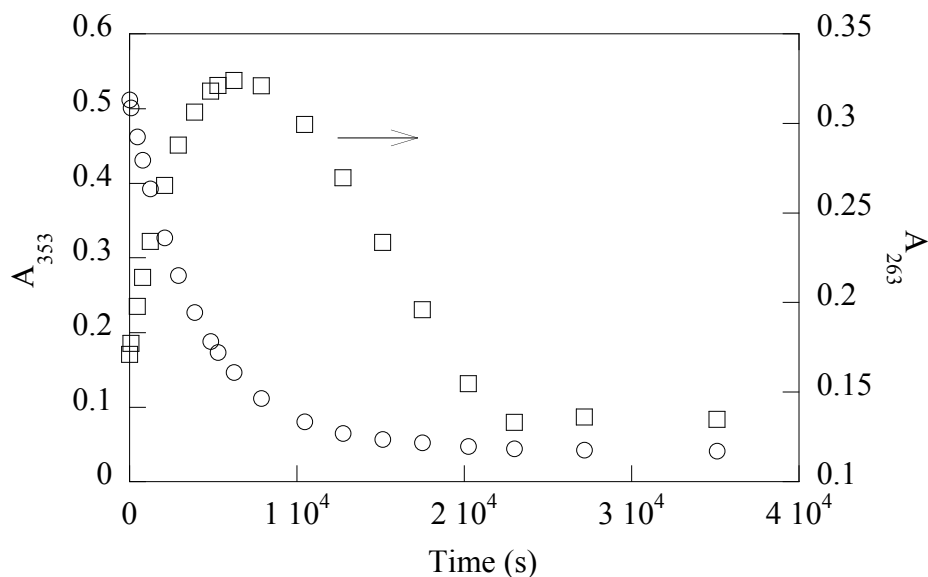


Figure 3-4: Absorption-time profile for decomposition of HDPT (3.2×10^{-5} M) in the presence of β -CD (7 mM) in 2% MeOH aqueous solution at pH 6.16 (0.05 M phosphate buffer), monitored at 353 nm (O) and 263 nm (□).

The time-resolved absorption spectra of CH_3ODPT in aqueous solutions at pH 6.16 were not recorded due to the fast decomposition of this substrate. However, as in the case of HDPT, the rate of decomposition of CH_3ODPT decreased significantly in the presence of β -CD, so that the corresponding time-resolved absorption spectra could be recorded (Figure 3-5). Although in the presence of β -CD, the λ_{max} (314 nm) ascribed to the diazonium ion $p\text{-CH}_3\text{O-C}_6\text{H}_4\text{N}_2^+$ is in excellent agreement with the reported λ_{max} value in aqueous media (*i.e.*, 315 nm¹⁰⁴). Formation of the C-azo compound was not observed, which is consistent with the fact that the *para* position of the phenyl ring is substituted with a $\text{CH}_3\text{O-}$ group.

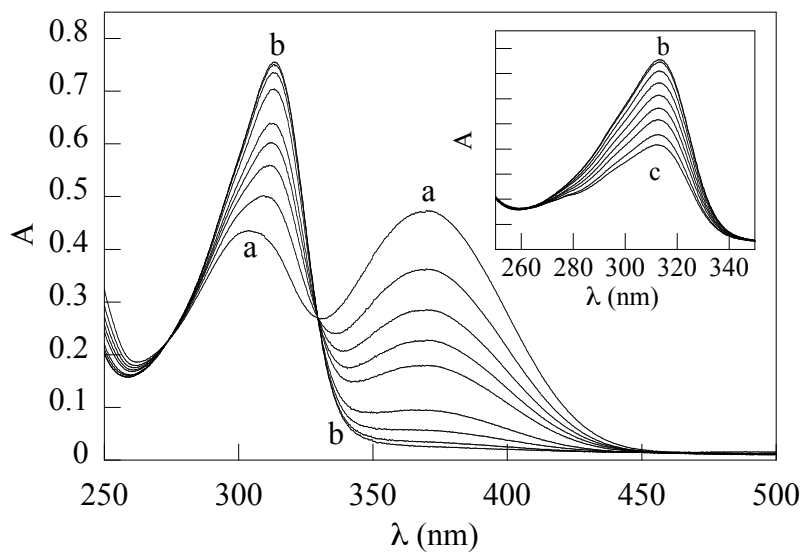


Figure 3-5. Time-resolved absorption spectra for decomposition of CH_3ODPT (2.9×10^{-5} M) in 2% MeOH aqueous solution at pH 6.16 (0.05 M phosphate buffer), obtained within 1 min and 16 min (from a to b) after sample preparation. Inset: corresponding spectra obtained within 16 min and 7.3 h (from b to c) after sample preparation.

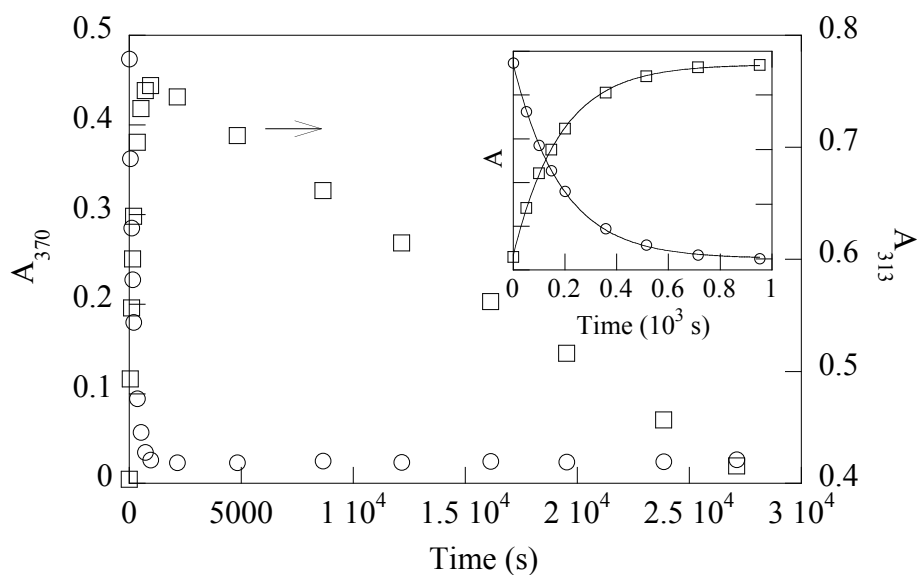


Figure 3-6. Absorption-time profile for decomposition of CH_3ODPT (2.9×10^{-5} M) in the presence of β -CD (7 mM) in 2% MeOH aqueous solution at pH 6.16 (0.05 M phosphate buffer), monitored at 353 nm (○) and 263 nm (□). Inset: expanded profiles obtained within first 17 min.

Series of solutions were made at different pHs in the absence (for both substrates) and presence (for CH₃ODPT) of β-CD, to determine the dependence of the rate of decomposition on proton concentration. The decomposition of HDPT was monitored at 352 nm while that of CH₃ODPT was monitored at 367 nm. In all cases, the kinetic traces followed a first order rate law. The corresponding rate constants (see Tables A-1 and A-2 in Appendix) were obtained by curve fitting to a first order rate law (see Experimental Section). The proton dependence of the acid-catalyzed decomposition rate constants for HDPT and CH₃ODPT in the absence and presence of β-CD is shown in Figures 3-7 and 3-8, respectively. For both substrates, the observed rate constant is directly proportional to proton concentration, even in the presence of β-CD; however, the higher the β-CD concentration, the smaller the slope of the line.

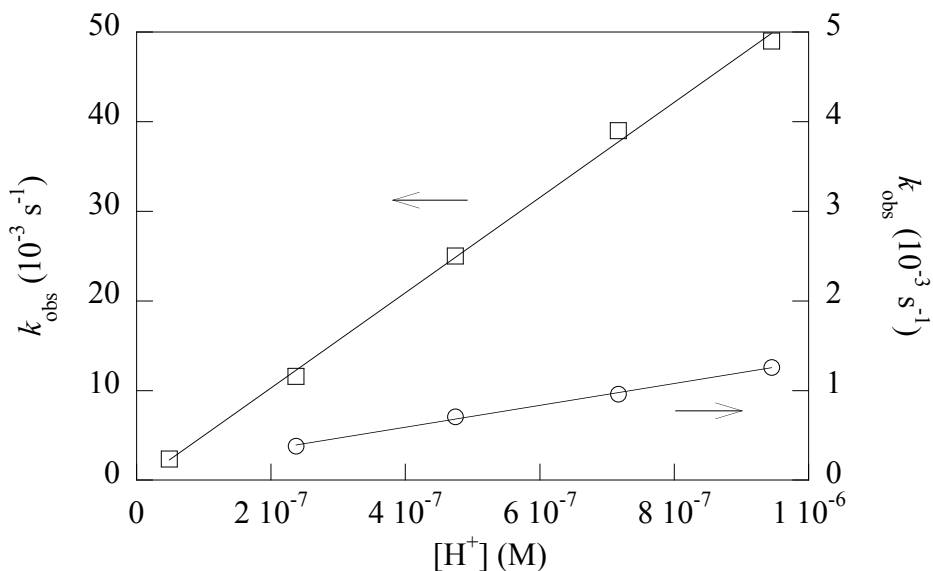


Figure 3-7. Proton dependence of the observed rate constant for acid-induced decomposition of HDPT (○) and CH₃ODPT (□) in 2% MeOH aqueous solutions.

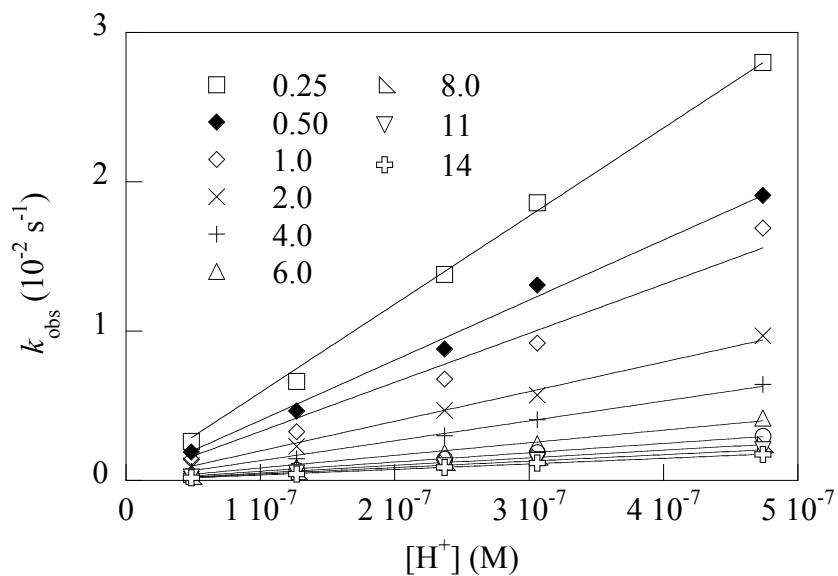


Figure 3-8. Proton dependence of the observed rate constant for acid-induced decomposition of CH₃ODPT in 2% MeOH aqueous solutions in the presence of varying amounts of β-CD (concentrations given in mM).

In order to determine if the inhibition effect observed in the presence of β-CD arises from unspecific interactions between triazenes and glucose additives or from formation of inclusion complexes, glucose and soluble starch as well as four other CDs were tested. Table 3-1 lists the observed rate constants for acid-induced decomposition of target triazenes upon addition of various glucose derivatives. The lack of any effect in the presence of 10 mM glucose and only a slight retardation (if at all significant) upon addition of soluble starch (equivalent to 2 mM β-CD in mass), as well as the CD dependent inhibition effects on the rate of decomposition of HDPT in aqueous solutions at pH 6.16, clearly indicates that the inhibition effects observed in the presence of CDs are due to the formation of inclusion complexes.

Table 3-1. Observed rate constants for decomposition of 1,3-diphenyltriazenes in 2% MeOH aqueous solutions at pH 6.16 in the presence of CDs or other glucose additives.^a

Additive	k_{obs} (10^{-3} s^{-1})		
	[Additive]	HDPT	MeODPT
None	0	1.26 ± 0.01	49 ± 3
D-Glucose	10 mM	1.24 ± 0.01	
Starch	2 mM ^b	1.00 ± 0.01	
α -CD	10 mM	0.117 ± 0.002	0.41 ± 0.01
β -CD	10 mM	0.204 ± 0.002	3.9 ± 0.1
HP- β -CD	10 mM	0.0452 ± 0.0001	0.800 ± 0.003
TM- β -CD	10 mM	0.0908 ± 0.0002	1.51 ± 0.05
TM- β -CD	4.3 mM	0.228 ± 0.001	3.74 ± 0.02
γ -CD	5 mM	0.998 ± 0.003	19.4 ± 0.1

^a $\mu = 0.5 \text{ M (NaCl)}$, $T = (21 \pm 0.1) \text{ }^\circ\text{C}$. ^bIn terms of β -CD equivalents.

In order to investigate the dependence of the inhibition effects on CD cavity size and rim substitution, for both substrates and each CD employed in this study, kinetic traces were recorded using series of solutions at pH 6.16 but varying host concentration. Figures 3-9 to 3-12 show the corresponding plots of observed rate constants (see Tables A-3 and A-4 in Appendix for values) of the two target triazenes vs. [CD]. As can be seen, the inhibition increases with increasing CD concentrations, and its strength is CD dependent.

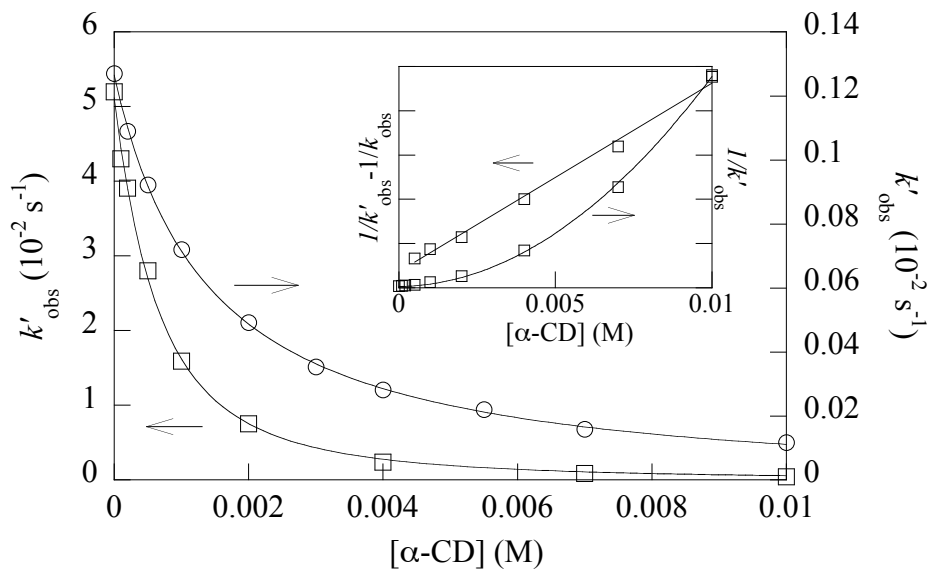


Figure 3-9. Influence of α -CD concentration on the observed rate constant for acid-induced decomposition of HDPT (○) and CH_3ODPT (□) in 2% MeOH aqueous solution at pH 6.16 (0.05 M phosphate buffer).

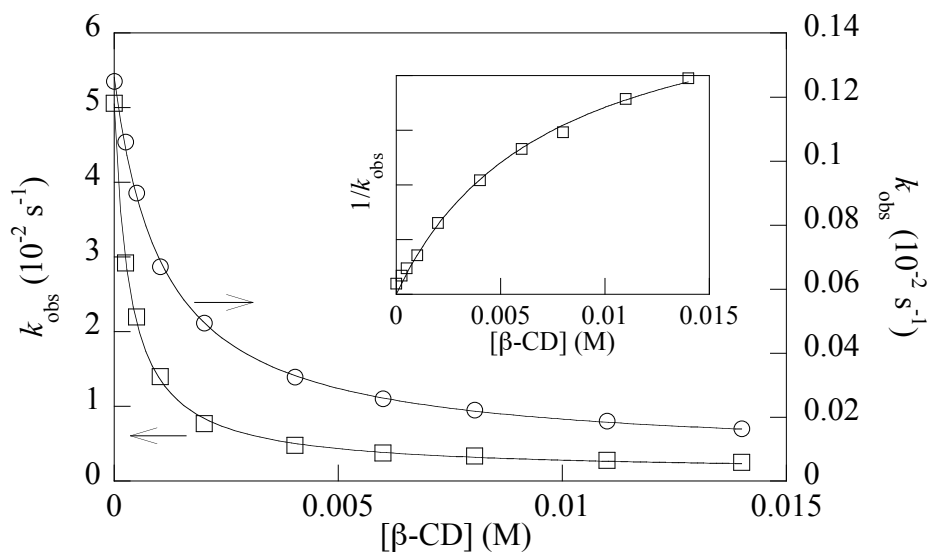


Figure 3-10. Influence of β -CD concentration on the observed rate constant for acid-induced decomposition of HDPT (○) and CH_3ODPT (□) in 2% MeOH aqueous solution at pH 6.16 (0.05 M phosphate buffer).

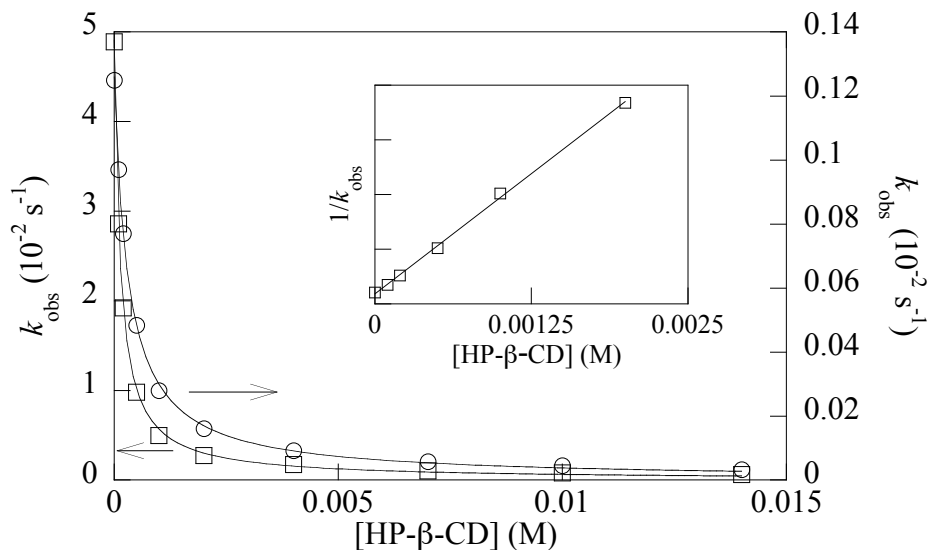


Figure 3-11. Influence of HP- β -CD concentration on the observed rate constant for acid-induced decomposition of HDPT (O) and CH₃ODPT (□) in 2% MeOH aqueous solution at pH 6.16 (0.05 M phosphate buffer).

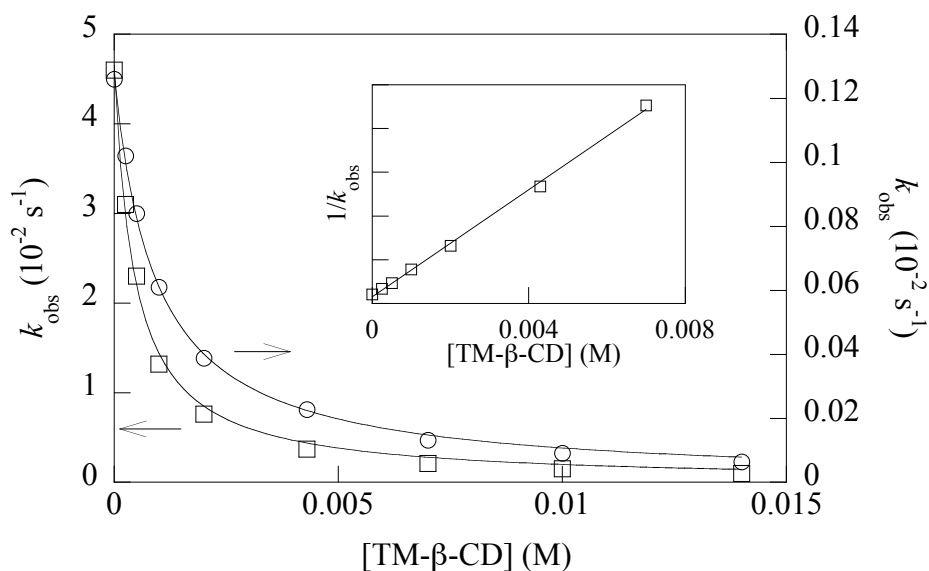


Figure 3-12. Influence of TM- β -CD concentration on the observed rate constant for acid-induced decomposition of HDPT (O) and CH₃ODPT (□) in 2% MeOH aqueous solution at pH 6.16 (0.05 M phosphate buffer).

Evidence of inclusion complexes formation is not only obtained from the kinetic study but it is also inferred from Figures 3-1 and 3-2, where absorption spectral changes are observed upon addition of β -CD. Further evidence is obtained from absorption titration spectra. Three sets of spectra were recorded using pH 9.98 borax buffer solutions (to diminish substrate decomposition): HDPT in the presence of α -CD and HP- β -CD, respectively, and CH₃ODPT in the presence of α -CD. Experiments with HDPT as substrate were carried out in 2% MeOH aqueous solutions, whereas those with CH₃ODPT were done in 2% MeCN aqueous solutions, due to its appreciable decomposition in MeOH within the time period needed for the experiments. Same as in the case of β -CD addition, a bathochromic shift in λ_{max} is observed for each set of titration experiments (Figures 3-13 and 3-14). For HDPT, the shift is *ca.* 8 nm for both α -CD and HP- β -CD, while for CH₃ODPT, addition of α -CD causes a shift of 12 nm. The absorption maximum for HDPT decreases upon addition of CDs, especially for α -CD addition. For CH₃ODPT, the intensity ultimately increases upon addition of α -CD.

Circular dichroism spectrometers record the absorption difference between left- and right-handed circularly polarized lights of an absorbing optically active substance.¹⁰⁵ Triazines are optical inactive, thus do not exhibit circular dichroism signals. CDs, in spite of being chiral compounds, do not have circular dichroism signals in the 200-1000 nm (UV-visible) region; however, they are capable of inducing circular dichroism when they form complexes with achiral compounds bearing chromophores.⁶⁴ Experiments to acquire ICD spectra of HDPT in the presence of CDs were carried out under the same condition as the UV-visible titration experiments, *i.e.*, pH 9.98 borax buffer aqueous solutions, to diminish the decomposition of the substrate. As shown in Figure 3-15, upon addition of

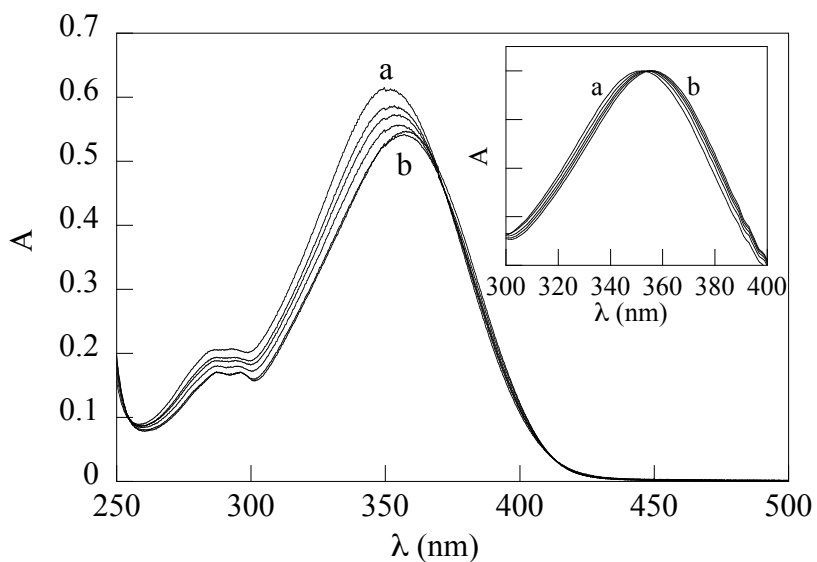


Figure 3-13. Absorption titration spectra of HDPT (3.8×10^{-5} M) with α -CD (0, 0.5, 1, 2, 7.5, and 21 mM from a to b) in 2% MeOH aqueous solutions at pH 9.98 (0.05 M borax buffer). Inset: normalized spectra for HDPT in the presence of HP- β -CD (0, 0.2, 0.5, 1, and 10 mM from a to b).

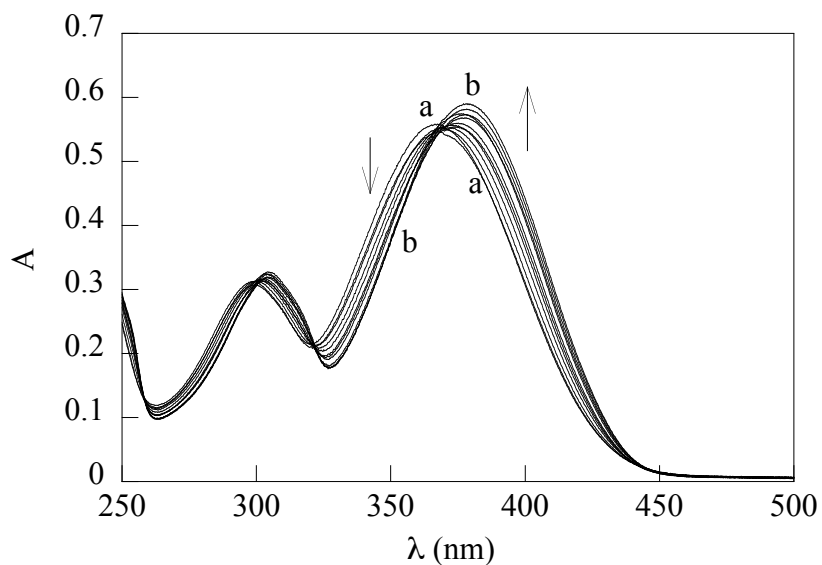


Figure 3-14. Absorption titration spectra of CH_3ODPT (3.5×10^{-5} M) with α -CD (0, 0.5, 1, 2, 3, 4, 5, 7.5, 10, 13.5, 17 and 21 mM from a to b,) in 2% MeCN aqueous solutions at pH 9.98 (0.05 M borax buffer).

α -CD, β -CD, HP- β -CD and TM- β -CD to HDPT containing solutions, different ICD spectra were recorded. These induced circular dichroism spectra are the best evidence of CD-triazene inclusion complex formation.

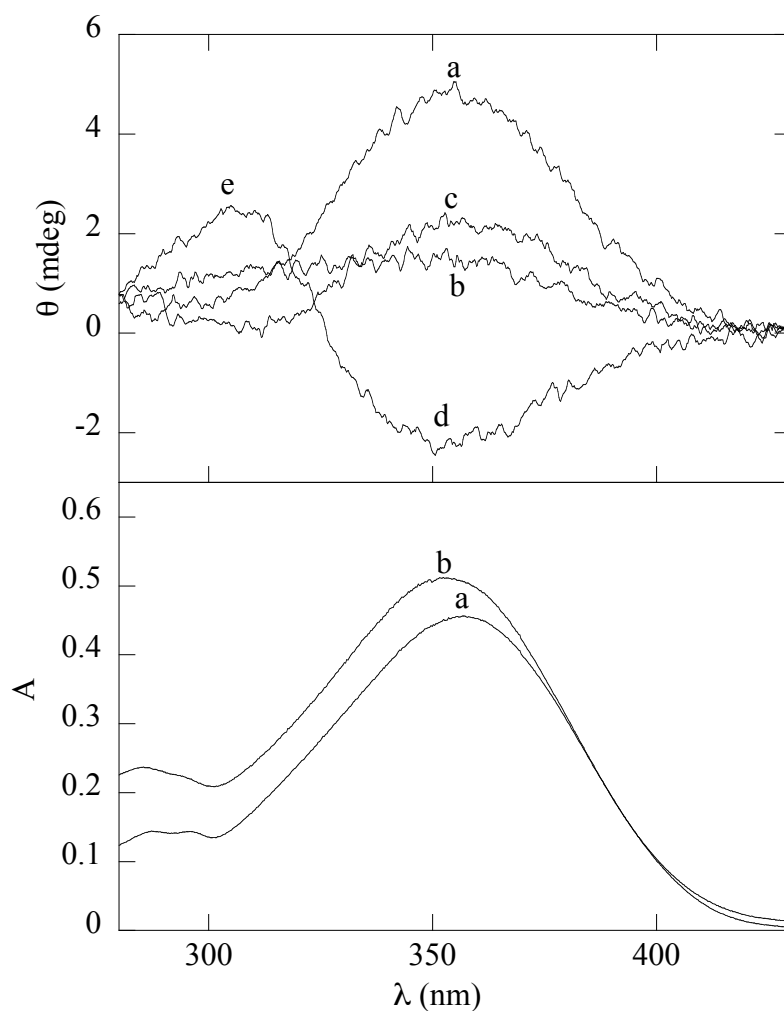


Figure 3-15. Induced circular dichroism (top) and absorption (bottom) spectra of HDPT (3.2×10^{-5} M) in the presence of CDs (7 mM): (a) α -CD; (b) β -CD; (c) HP- β -CD; (d) TM- β -CD.

The ICD titration spectra of HDPT with α -CD were obtained by keeping the concentration of HDPT at 3×10^{-5} M while that of α -CD ranged from 0 to 21 mM. The ICD signal grows with increasing α -CD concentration up to 7.5 mM, and then remains in that level with higher α -CD concentration (Figure 3-16).

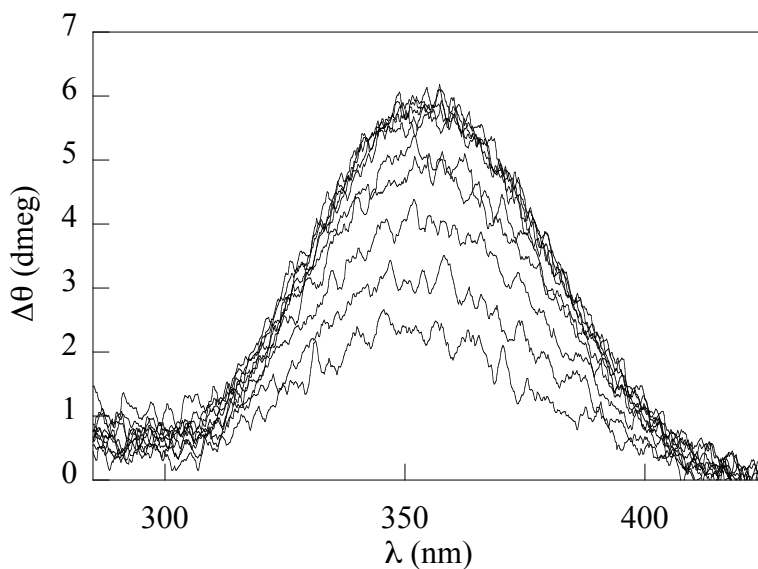
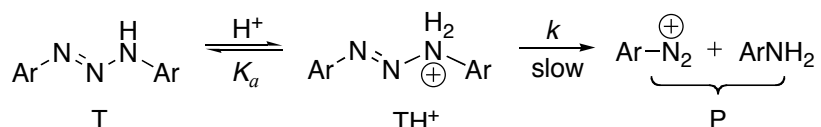


Figure 3-16. Induced circular dichroism titration spectra of HDPT (3×10^{-5} M) with α -CD (0.5, 1, 2, 3, 4, 5, 7.5, 10, 17 and 21 mM, from bottom to top) in 2% MeOH aqueous solutions at pH 9.98 (0.05 M borax buffer).

It should be pointed out here that, for UV-visible and ICD titration experiments, solutions with α -CD concentrations larger than 21 mM could not be used due to aggregation of α -CD in solution. Native CDs are known to aggregate in solution, which may make the solutions hazy.¹⁰⁶ As a consequence, the light beam of the spectrometer is dispersed when passing through the solution and false signals are recorded.

3.2 Discussion

The acid-catalyzed decomposition of 1,3-diphenyltriazene under experimental conditions analogous to those of this study has been interpreted in terms of specific acid catalysis, since the rates of decomposition increase with decreasing pH while are independent of buffer concentration.^{90a} Scheme 3-1, in which T, TH⁺, *k*, and *K_a* represent the triazene, the N³ protonated triazene, the first order rate constant for N²-N³ bond cleavage, and the acid dissociation equilibrium constant for TH⁺, respectively, illustrates the mechanism for specific acid-catalyzed triazene decomposition. The corresponding expression of the observed rate constant (*k_{obs}*) is given by Eq. 3-1.



Scheme 3-1. Specific acid-catalyzed decomposition mechanism for 1,3-diphenyltriazenes.

$$k_{obs} = \frac{k[\text{H}^+]}{K_a + [\text{H}^+]} \quad \text{Eq. 3-1}$$

The linear plots of *k_{obs}* vs. proton concentration (Figure 3-7) indicate that, under the experimental conditions of this study, the [H⁺] term in the denominator of Eq. 3-1 is negligible. Instability of triazenes in acidic media precludes spectral titrations for measurement of their *K_a* values. The reported *pK_a* value for the N³ protonated parent triazene as determined from the dependence of the first order rate constant on pH is 4.95.³ Resonance effects in 1,3-diphenyltriazenes are expected to decrease the electron density

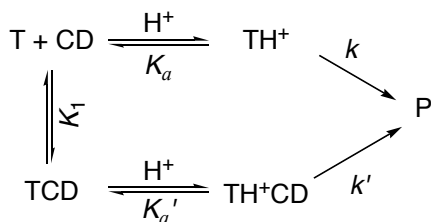
of the triazeno moiety, and hence the basicity, and as a consequence to increase the acidity of its conjugated acid TH^+ . Thus, one would expect the pK_a value of TH^+ to be smaller than 4.95, *i.e.*, much smaller than the lowest pH (6.16) in this study. On the other hand, the electron-withdrawing character of the $-\text{N}=\text{N}-\text{Ar}$ group^{50c} would render the N^3 -protonated forms of HDPT and CH_3ODPT more acidic than the conjugate forms of the corresponding aniline, *i.e.*, anilinium ($pK_a = 4.63^{107a}$) and *p*-anisidinium ions ($pK_a = 5.34^{107b}$), hence the K_a values of the TH^+ species would be much smaller than the lowest pH (6.16) in this study.

The linear plots in Figure 3-7 yield second-order rate coefficient k/K_a (slope) values of $(5.26 \pm 0.07) \times 10^4 \text{ M}^{-1}\text{s}^{-1}$ and $(1.36 \pm 0.04) \times 10^3 \text{ M}^{-1}\text{s}^{-1}$ for CH_3ODPT and HDPT, respectively. These values are in good agreement with values from other independent experiments, *i.e.*, $(5.90 \pm 0.08) \times 10^4 \text{ M}^{-1}\text{s}^{-1}$ for CH_3ODPT (value calculated from the top line of Figure 3-8*) and $(1.37 \pm 0.03) \times 10^3 \text{ M}^{-1}\text{s}^{-1}$ for HDPT.^{90a} CH_3ODPT has a much larger second-order rate coefficient value than HDPT, which is consistent with previous reports on the substituent effects on the acid-induced decomposition of aryltriazenes.^{11,108-110} The trend is attributed to an increase in the basicity of the amino N and in the stability of diazonium ion, with increasingly stronger electron-donating groups.

The inhibition effect of CDs on the acid-induced decomposition of triazenes rises from inclusion complex formation. The most commonly claimed stoichiometric ratio for CDs complexes is 1:1,¹¹¹ thus, the reaction scheme for decomposition of triazenes in the presence of CDs can be illustrated as shown in Scheme 3-2, in which TCD and TH^+CD

*Ionic strength kept at 0.55 M (NaCl)

represent the CD inclusion complex for triazene and TH^+ , respectively; k' and K_a' represent the first order rate constant for cleavage of the $\text{N}^2\text{-N}^3$ bond and the acid dissociation equilibrium constant for complexed TH^+ , respectively. Bearing in mind that, under the experimental conditions of this study, target substrates are essentially in their neutral form (*i.e.*, molar fraction of neutral substrate ≈ 1 , as inferred from Figure 3-8), the expression for the observed rate constant corresponding to Scheme 3-2 would be given by Eq. 3-2.



Scheme 3-2. Mechanism for specific acid-catalyzed decomposition of 1,3-diphenyl-triazenes in the presence of CDs.

$$k_{obs} = \left(\frac{k / K_a + k' / K_a' K_1 [\text{CD}]}{1 + K_1 [\text{CD}]} \right) [\text{H}^+] \quad \text{Eq. 3-2}$$

Values of k_{obs} as a function of β -CD concentration (Figure 3-10) for the two substrates can be well fitted with Eq. 3-2. The values of the different parameters determined through curve fitting according to Eq. 3-2 are listed in Table 3-2.

Table 3-2. First order rate coefficients and association equilibrium constants obtained for decomposition of HDPT and CH₃ODPT in the presence of CDs.^a

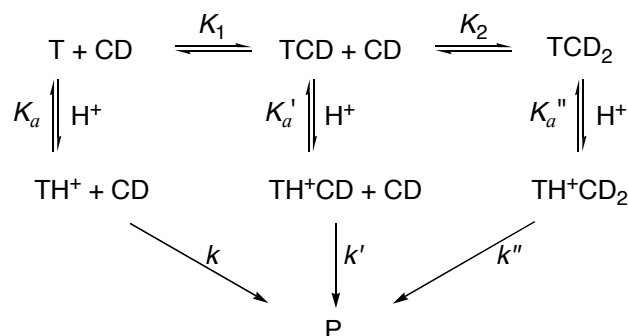
CD	HDPT			CH ₃ ODPT		
	$k[\text{H}^+]/K_a$ (10 ⁻³ s ⁻¹)	K_1 (10 ² M ⁻¹)	K_1K_2 (10 ⁵ M ⁻²)	$k[\text{H}^+]/K_a$ (10 ⁻³ s ⁻¹)	K_1 (10 ² M ⁻¹)	K_1K_2 (10 ⁵ M ⁻²)
α-CD	1.26 ± 0.01	7.4 ± 0.2	0.30 ± 0.05	51.2 ± 0.8	14 ± 2	7 ± 2
α-CD ^b				36.3 ± 0.1	4.0 ± 0.8	1.4 ± 0.4
β-CD	1.26 ± 0.01 (0.077 ± 0.009) ^c	9.1 ± 0.4		50.5 ± 0.5 (1.1 ± 0.2) ^c	29 ± 1	
HP-β-CD	1.26 ± 0.01	32.1 ± 0.8		49.1 ± 0.4	77 ± 2	
TM-β-CD	1.28 ± 0.01	10.9 ± 0.4		46.5 ± 0.9	22 ± 1	

^a 2% MeOH (v/v) aqueous solutions (unless stated otherwise); T = 21 °C; μ = 0.5 (NaCl); pH = 6.16 (0.05 M phosphate buffer). Errors given correspond to the standard deviations. ^b 2% MeCN (v/v) aqueous solutions. ^c Value for $k'[\text{H}^+]/K_a'$.

For HP- β -CD and TM- β -CD, curve fittings according to Eq. 3-2 lead to a negligible $k'/K'_a K_1[CD]$ term, which agrees well with the linear plots in Figures 3-11 and 3-12 insets. Thus, Eq. 3-2 can be reduced to Eq. 3-3, and the corresponding k/K_a and K_1 values obtained from curve fittings for HP- β -CD and TM- β -CD are also shown in Table 3-2.

$$k_{obs} = \frac{k/K_a}{1 + K_1[CD]}[H^+] \quad \text{Eq. 3-3}$$

For α -CD as host, neither Eq. 3-2 nor Eq. 3-3 fit plots of k_{obs} as a function of α -CD concentration. As illustrated in the inset of Figure 3-9, plots of $1/k_{obs}$ curve upward, which implies a higher order complex formation. The fact that in the UV-visible absorption titration spectra (Figures 3-13 and 3-14) no isosbestic point remains throughout the α -CD concentration range, suggests the existence of more than two stoichiometric states, in support of the involvement of higher order complexes. Formation of 2:1 (host:guest) inclusion complexes is a common observation when using α -CD as host molecule.¹¹² Scheme 3-3 shows the corresponding reaction mechanism, in which K_a'' and k'' represent the acid dissociation equilibrium constant and the first-order rate constant for heterolytic cleavage of 2:1 CD:TH⁺ complexes.



Scheme 3-3. Mechanism for specific acid-catalyzed decomposition of 1,3-diphenyl-triazenes in the presence of CDs (with formation of higher order complexes).

The expression of the observed rate constant corresponding to Scheme 3-3 is given by Eq. 3-4. However, curve fittings according to Eq. 3-4 of data in Figure 3-9 reveal that the $(k'/K_a'K_1[\text{CD}] + k''/K_a''K_1K_2[\text{CD}]^2)$ term in the numerator is negligible in comparison to the k/K_a term, which is consistent with the fact that plots of $(1/k'_{obs} - 1/k_{obs})/[\text{CD}]$ vs. $[\text{CD}]$ are linear (Figure 3-9 inset). Thus, Eq. 3-4 can be reduced to Eq. 3-5, from which nonlinear fittings yield association equilibrium constants for 1:1 and 2:1 α -CD complexes (Table 3-2).

$$k'_{obs} = \left(\frac{k/K_a + k'/K_a'K_1[\text{CD}] + k''/K_a''K_1K_2[\text{CD}]^2}{1 + K_1[\text{CD}] + K_1K_2[\text{CD}]^2} \right) [\text{H}^+] \quad \text{Eq. 3-4}$$

$$k_{obs} = \frac{(k/K_a)[\text{H}^+]}{1 + K_1[\text{CD}] + K_1K_2[\text{CD}]^2} \quad \text{Eq. 3-5}$$

In all cases, the k/K_a values determined from curve fittings of the observed rate constant obtained in the presence of CDs (Table 3-2) are in good agreement with the

values determined from the pH dependent series in the absence of CD. Furthermore, the value of $(k/K_a + k'/K'_a K_1[\text{CD}])/(1 + K_1[\text{CD}])$ calculated from Table 3-2 for HDPT in the presence of 11 mM β -CD is *ca.* $195 \text{ M}^{-1}\text{s}^{-1}$, in excellent agreement with the value previously obtained by our group, namely $196 \pm 8 \text{ M}^{-1}\text{s}^{-1}$, by measuring observed rate constants as a function of pH in the presence of 11 mM β -CD.¹¹³

As described in Section 1.2.2, non-covalent catalysis by CDs can be attributed to two effects: conformational and microsolvant effects. The inhibition by CDs of the acid-catalyzed decomposition of triazenes can be rationalized in terms of microsolvant effects. As mentioned in Section 1.1.3.2, the acid-induced decomposition of 1,3-diphenyl-triazenes has been shown to be solvent sensitive; the overall trend is that the decomposition rate decreases with decreasing solvent polarity. From previous studies in our research group, the k/K_a values in 30% THF aqueous solutions are $(21.3 \pm 0.7) \text{ M}^{-1}\text{s}^{-1}$ and $(976 \pm 9) \text{ M}^{-1}\text{s}^{-1}$ for HDPT and CH_3ODPT , respectively,¹¹ which are much smaller than those obtained in 2% MeOH aqueous solutions (listed in page 59). Protonation constants for anilines in dioxane-water mixtures have been shown to systematically decrease as the concentration of dioxane increases.¹¹⁴ Thus, K_a values for TH^+ are expected to be smaller in 2% MeOH than in 30% THF. According to the Hughes and Ingold theory, the rate of reactions for which the charge density in the activated complex is lower than in the initial reactant will decrease (to a small extent) with increasing solvent polarity.^{97b} Thus, k values are expected to increase (slightly) with increasing organic co-solvent fraction, since the transition state for the heterolytic cleavage of TH^+ involves charge dispersion. The significant decrease in reactivity on going from 2% MeOH to 30% THF indicates that the rate of decomposition of target triazenes is

dominated by their basicity. As indicated in Section 1.2, CDs are macrocyclic molecules with hydrophobic cavities. Thus, when triazenes are encapsulated in the CDs cavity, the N^3 protonation constant would be decreased. As a consequence, the k/K_a value is decreased and the decomposition is inhibited.

As shown in Table 3-2, among all four CDs involved in this study, β -CD is the only one for which the reactivity of the TH^+CD is detected, which suggests that guest triazenes experience less environmental changes upon inclusion in β -CD than upon inclusion in the narrower α -CD or in any of the β -CD derivatives (in which alkyl substituents elongate the cavity and increase the hydrophobicity of its edges^{115,116}). From Table 3-1, it can be seen that with 5 mM γ -CD there is barely any inhibition on triazenes decomposition. As shown in Table 1-1, among the three native CDs, γ -CD has the largest cavity size and accommodates the highest number of water molecules in its cavity. Hence, the lack of inhibition by γ -CD on triazenes decomposition might be attributed to the triazene molecule experiencing a predominantly aqueous environment when included in γ -CD.

The K_1 values (Table 3-2) derived from the dependence of observed rate constants as a function of [CD] increase in the order α -CD < β -CD ~ TM- β -CD < HP- β -CD. This is consistent with the trend for binding constants reported for complexation with aromatic molecules, *i.e.*, α -CD < β -CD^{111,112} and β -CD < β -CD derivatives.^{65,116} The K_1 values for CH_3ODPT are *ca.* twice as large as those of $HDPT$, and the values obtained from β -CD are comparable to the literature values for inclusion of azobenzene derivatives (X -Ph-N=N-N(CH_3)₂⁺Cl⁻), which are 860 M⁻¹ and 1300 M⁻¹ for X = H and CH₃, respectively.¹¹⁶

ICD spectra can help to elucidate the relative orientation of triazenes in CDs. The sign of the ICD signal depends on the orientation the guest molecules take in the inclusion complex, while the intensity of the signal depends not only on the orientation, but also on the strength of the interaction between the host and guest molecules.¹¹⁷ According to the empirical rules on the ICD phenomena on CD complexes, the ICD of a chromophore located inside the cyclodextrin cavity will be positive when its electric transition dipole moment is parallel to the principal axis of the cyclodextrin, while the ICD will be negative when the alignment inside the cavity is perpendicular to the principal axis of the host; reverse ICD signals will be expected when the chromophore is located outside the cavity.¹¹⁸⁻¹²⁰

The single positive signal centered at ~350 nm for α -CD, β -CD and HP- β -CD inclusion complexes with HDPT is attributed to the π - π^* transition band of the N=N group being nearly parallel to the axial direction of the CDs, *i.e.*, the N=N group is aligned parallel to the principal axis. This conclusion is in agreement with the reported orientation for *para*-substituted azobenzene derivatives, *i.e.*, the linear molecules penetrate CDs cavity with the N=N group located in the centre of and parallel to the chiral cavity.¹²¹⁻¹²³

For TM- β -CD inclusion complexes with aromatic azo dyes, split pattern of signals is very common.^{121,124,125} Methylation of the hydroxyl groups reverse the CD hydrophobicity, *i.e.*, the most hydrophobic surface regions are located at the torus rims made up by the 2-, 3- and 6-OMe groups,¹¹⁵ as a result, the N=N group moves from the centre of the cavity to the rim, but still parallel to the cavity axis.¹²⁵ Thus, rules for signal signs reverse; the sign of the 350 nm absorption band would be negative. The positive

signal at the shorter wavelength (which corresponds to the shoulder in the absorption spectra) might arise from the observed π - π^* transition of the phenyl ring being parallel to the principal axis of TM- β -CD.¹¹⁹

The UV-visible and ICD titration spectra presented in Figures 3-13, 3-14 and 3-16 were recorded in an attempt to measure binding constants. The changes (ΔI) observed in absorbance and in ellipticity as a function of CD concentration can be related to the binding constant(s) of Schemes 3-2 and 3-3 according to Eq. 3-6 and 3-7, respectively,

$$\Delta I = \frac{\Delta c_1 b K_1 [CD] [T]_0}{1 + K_1 [CD]} \quad \text{Eq. 3-6}$$

$$\Delta I = \frac{\Delta c_1 b K_1 [CD] [T]_0 + \Delta c_2 b K_1 K_2 [CD]^2 [T]_0}{1 + K_1 [CD] + K_1 K_2 [CD]^2} \quad \text{Eq. 3-7}$$

where Δc_1 and Δc_2 represent, respectively, the difference between molar extinction coefficients or molar ellipticities for 1:1 or 2:1 (host:guest) complexed and free triazenes; $[T]_0$ refers to total triazene concentration.

Due to the limited number of ΔI values obtained, and in the case of UV-visible experiments the small ΔA values recorded ($\Delta A < 0.1$), a statistically significant fitting according to Eq. 3-7 to determine the corresponding binding constants was precluded. However, when one of the binding constants was fixed to the value obtained from the kinetic experiments, the one determined from Eq. 3-7 was of the same order as the value obtained from the kinetic study. Furthermore, fittings of ΔA values (obtained from

Figures 3-13 and 3-14) according to Eq. 3-6 render wavelength dependent K_1 values; this result also provides clear experimental evidence for higher-order complexes formation.

During the UV-visible titration experiments for CH₃ODPT, it was observed that for any given α -CD concentration, the spectral changes recorded in 2% MeOH were always larger than those in 2% MeCN, which suggests lower binding constants in the latter system. It is well established that binding properties of CDs can be significantly affected by the presence of aprotic organic cosolvents; competition for the CD cavity between guest and co-solvent may lead to a significant decrease in equilibrium constants.^{116,126} Among all the organic solvents, MeOH resembles the structure and properties of water the most, while MeCN is an aprotic organic solvent and hence, more competitive for CD complexation. In order to verify the suggestion that the binding constant between CH₃ODPT and α -CD is higher in 2% MeOH than in 2% MeCN, observed rate constants for CH₃ODPT decomposition were determined in 2% MeCN aqueous solutions.¹¹³ From the dependence of the observed rate constants on α -CD concentration, lower equilibrium constants in comparison with values for 2% MeOH were obtained (Table 3-2). In addition, the k/K_a value obtained in 2% MeCN (Table 3-2) is smaller than that in 2% MeOH, which is in good agreement with the dependence of the reaction on solvent polarity mentioned in page 64.

3.3 Conclusions

Formation of inclusion complexes between cyclodextrins and triazenes has an inhibitory effect on the rate of acid-induced decomposition of 1,3-diphenyltriazenes. This inhibition is ascribed to the decrease in basicity of the amino N, as a result of the apolar

nature of the CD cavity (a microsolvant effect). The strength of the inhibition depends not only on the size of the CD cavity, but also on the substituents on the cavity rims. Binding constants for 1:1 host:guest complexes increase in the order α -CD < β -CD ~ TM- β -CD < HP- β -CD, with values for CH₃ODPT being larger than those for HDPT. The orientation of the guest triazine molecules in the CD cavity depends on the substituents on the cavity rims.

Chapter 4. Experimental

4.1 Reagents and instruments

The triazene substrates HDPT, CH₃ODPT and CF₃DPT were existing samples from previous studies.^{10,14} The melting points of these triazenes were measured on a Mel-temp II apparatus: HDPT 98-100 °C (dec.) (lit.^{1a} 100 °C (dec.)), CF₃DPT 115-116°C (dec.) (lit.¹²⁷ 115 °C (dec.)), CH₃ODPT 97-98 °C (dec.), (lit.¹²⁸ 98-100 °C (dec.)). Boric acid and D-glucose (Baker), NaOH, Na₂HPO₄, KH₂PO₄ and potassium hydrogen phthalate (BDH), NaCl and soluble starch (EM Science), AgNO₃, HgCl₂, α-CD, β-CD, γ-CD and TM-β-CD (Aldrich), and HP-β-CD (TCI) were all analytical grade reagents and used as received. MeOH and MeCN (OmniSolv, EM science) were used as received; THF (ACS, EM science) was distilled before use. Ultra pure water obtained from a Millipore Milli-Q apparatus was used to prepare the aqueous solutions.

Buffer pH values were determined with an ATI Orion PerpHecT 350 digital pH meter using a glass body pH electrode. UV-visible spectra and kinetic traces were recorded with a Varian Cary 1 Bio UV-visible spectrophotometer (connected to a VWR Scientific Model 1160A circulating water bath) using 1 cm quartz cells; a few absorption spectra were recorded on an Agilent 8542 UV-visible spectrophotometer. Induced circular dichroism spectra were recorded on a JASCO J-715 spectropolarimeter (0.2 nm step resolution, 10 accumulations) using 1 cm quartz cells.

4.2 Laser flash photolysis (LFP)

LFP is a powerful tool for characterization of photochemical and photophysical processes, by combining the information obtained from transient absorption spectra and

kinetic traces.⁹⁵ A LFP spectrometer is composed of a sample cell holder, a xenon lamp (monitoring source), laser (excitation source), optical quality lenses and filters, monochromator/photomultiplier tube (MC/PMT, detector), and analysis devices including digitizer, synchronizer, distribution box and computer (Figure 4-1).⁹⁵

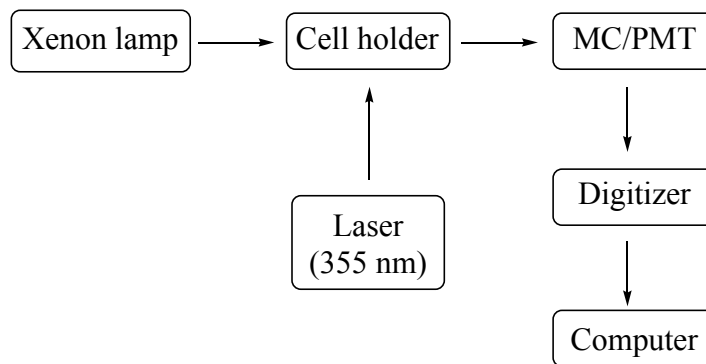


Figure 4-1. Laser flash photolysis apparatus diagram

The laser employed in our system is a nanosecond Neodymium-Yttrium Aluminum Garnet (Nd-YAG) laser operating at 355 nm (266 nm and 532 nm are also available). It is capable of generating high-energy laser pulses (< 10 mJ/pulse, 4-6 ns pulses), which can easily promote the ground state molecules to excited states. The beam from the xenon lamp is used as the monitoring beam, and the MC/PMT detector detects the light not being absorbed by the sample before and after laser excitation, so then the difference in absorbance (ΔA) is recorded.

Kinetic traces are obtained by monitoring ΔA at a chosen (monitoring) wavelength as a function of time (Figure 4-2), and are used to follow the evolution of transient species. The monitoring wavelength usually is determined from transient absorption spectra, which are plots of ΔA as a function of wavelength. The observed kinetic traces lead to

values of rate constants by proper kinetic fittings. Three possible types of time-resolved signals are shown in Figure 4-2: (1) $\Delta A > 0$, when the transient species absorb more than the precursors do; (2) $\Delta A = 0$, when the transient species have the same absorbance as the precursors have; (3) $\Delta A < 0$, when the transient species absorb less than the precursors do. In the case of triazenes, the kinetic traces (monitored at 390 nm) are as trace (3) in Figure 4-2, since target *cis*-triazenes absorb less than the *trans*-forms at $\lambda > 350$ nm.¹²⁹

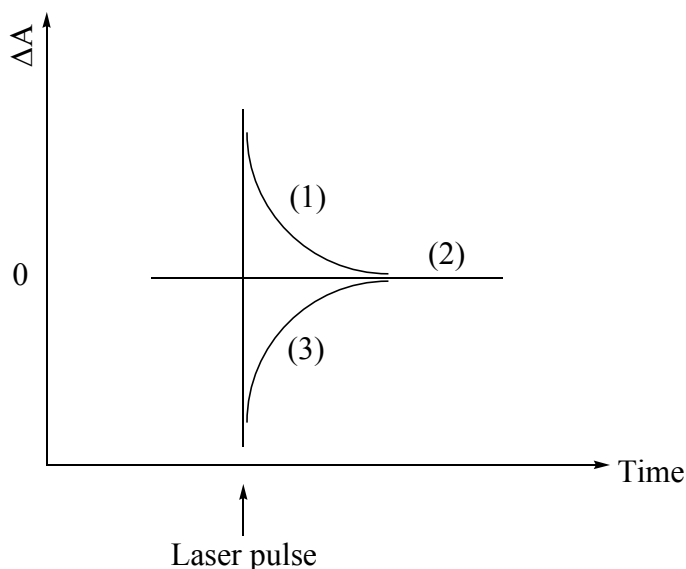


Figure 4-2. Possible kinetic traces observed with a LFP system.

4.3 Preparation of solutions

Borax buffer solutions were prepared from a stock NaOH aqueous solution and boric acid. The stock NaOH aqueous solution was standardized against potassium hydrogen phthalate. Phosphate buffer solutions were made from Na_2HPO_4 and KH_2PO_4 . The pH values of the buffer solutions were determined before substrate triazene was added.

All solutions for metal-triazene complexes studies were kept at room temperature (*i.e.*, (21 ± 1) °C). Sample solutions for spectral titration experiments were made from two stock solutions: triazene stock solution in organic cosolvent-aqueous borax buffer (or NaOH) and (concentrated) metal cation stock aqueous solution. Series of solutions at constant triazene concentration and variable metal cation concentration were prepared by mixing a constant aliquot of the triazene stock solution and different amounts of the metal cation stock solution (transferred with a μL syringe) in individual volumetric flasks, before diluting with water to the mark. The concentration of the triazene stock solution was adjusted so that after dilution, the final triazene concentration was *ca.* 1.5×10^{-5} M or *ca.* 3×10^{-5} M, depending on the solubility of the metal-triazene complex. The final total buffer concentration of sample solutions in borax buffer was 0.05 M.

Sample solutions for Job's method experiments were prepared from stock triazene and metal cation solutions having the same solute concentration and solvent composition. Thus, series of solutions at constant total triazene plus metal cation concentrations but with different $[\text{triazene}]/[\text{metal cation}]$ ratios were prepared by mixing aliquots of the two stock solutions in different ratios, while keeping the sum of the two aliquots constant, in individual volumetric flasks before diluting with water to the mark.

For the LFP experiments, sample solutions were made in individual volumetric flasks as follows: to a constant aliquot of a stock buffer or NaOH aqueous solution, organic cosolvent was added (if at all needed), followed by slow addition of a small aliquot (using a μL syringe) of a concentrated triazene stock solution in MeOH, and then addition of the corresponding aliquot (also using a μL syringe) from a concentrated metal cation stock aqueous solution, and finally diluting with water to the mark. It should be noted that the

order in which the aliquots from the different stock solutions are mixed is very important to avoid precipitation; the above order proved to be the best way to prepare solutions. The final total buffer concentration of sample solutions in borax buffer was 0.05 M. The absorbance at 355 nm of the sample solutions (which were contained in 0.7 cm quartz cells) typically ranged between 0.1 and 0.15 (with total triazene concentration in the order of $1.5\text{--}1.9 \times 10^{-5}$ M). All measurements were done at room temperature (*i.e.*, (21 ± 1) °C) using air-equilibrated samples.

Sample solutions for acid-catalyzed decomposition studies were prepared by adding 41 μL of a stock MeOH solution (unless stated otherwise) of the triazene to 2 mL of the buffer solution containing all other components. The resulting triazene concentration ranged between 1.9×10^{-5} M and 3.8×10^{-5} M. The ionic strength of the buffer was set at 0.5 M (unless stated otherwise), using NaCl as compensating electrolyte. β -CD solutions at a concentration higher than 10 mM and α -CD solutions at a concentration higher than 13.5 mM were heated at *ca.* 80°C for 30 minutes and cooled down before use. Sample solutions for absorption spectra were kept at room temperature (*i.e.*, (21 ± 1) °C), those for kinetic studies were kept at (21 ± 0.1) °C using a circulating water bath, and those for ICD experiments were kept at (24 ± 1) °C (ambient temperature of the biochemistry laboratory).

4.4 Kinetic data acquisition and processing

Kinetic traces for acid-catalyzed decomposition of triazenes were obtained either by using the automatic kinetic data acquisition function of the Varian UV-visible spectrometer to monitor the change in absorbance at the corresponding λ_{max} or by

manually reading the absorbance at λ_{\max} from the recorded time-resolved absorption spectra. The monitoring wavelengths were 352 and 367 nm for HDPT and CH₃ODPT, respectively. All reactions were followed until at least 80-90% decomposition of the starting substrate was observed. Observed rate constants (k_{obs}) were obtained by fitting the kinetic traces to a single exponential function (Eq. 4-1), in which A_t is the absorbance at time t , A_e is the absorbance at the end of the reaction, and A_0 is the initial absorbance. All reactions were measured at least twice, and resulting average observed rate constant values are listed in the Appendix.

$$A_t = (A_0 - A_e)\exp(-k_{\text{obs}} \times t) + A_e \quad \text{Eq. 4-1}$$

Proton concentrations were obtained from Eq. 4-2, using 0.732 as value for the proton activity coefficient γ_{H^+} .^{130a} This value is for γ_{H^+} in pure water; however, it has been reported that addition of up to 12% (v/v) MeOH has a negligible effect on γ_{H^+} .^{130b}

$$[\text{H}^+] = \frac{10^{-\text{pH}}}{\gamma_{\text{H}^+}} \quad \text{Eq. 4-2}$$

All curve fittings were carried out by using the general curve fitting procedure of Kaleidagraph™ software (Version 3.6.4) from Synergy Software.

References

- (1) Benson, F. R. *The High Nitrogen Compounds*; Wiley: New York, 1984; a) Ch. 2; b) Ch. 3.
- (2) Hayon, E.; Simic, M. *J. Am. Chem. Soc.* **1972**, *94*, 42-47.
- (3) Sutherland, J. W. *J. Phys. Chem.* **1979**, *83*, 789-795.
- (4) Le Fèvre, R. J. W.; Liddicoet, T. H. *J. Chem. Soc.* **1951**, 2743-2747.
- (5) Baro, J.; Dudek, D.; Luther, K.; Troe, J. *Ber. Bunsenges. Phys. Chem.* **1983**, *87*, 1155-1161.
- (6) Dugave, C.; Demange, L. *Chem. Rev.* **2003**, *103*, 2475-2532.
- (7) Delaire, J. A.; Nakatani, K. *Chem. Rev.* **2000**, *100*, 1817-1845.
- (8) Knoll, H. In *CRC Handbook of Organic Photochemistry and Photobiology*; Horspool, W. M., Lenci, F., Eds.; CRC Press: Boca Raton, 2004; Ch. 89.
- (9) Yager, K. G.; Barret, C. J. *J. Photochem. Photobiol. A: Chem.* **2006**, *182*, 250-261.
- (10) Barra, M.; Chen, N. *J. Org. Chem.* **2000**, *65*, 5739-5744.
- (11) Chen, N.; Barra, M.; Lee, I.; Chahal, N. *J. Org. Chem.* **2002**, *67*, 2271-2277.
- (12) Barra, M.; Srivastava, S.; Brockman, E. *J. Phys. Org. Chem.* **2004**, *17*, 1057-1060.
- (13) Zhang, H.; Barra, M. *J. Phys. Org. Chem.* **2005**, *18*, 498-503.
- (14) Barra, M.; Lim, H. *Trends Org. Chem.* **2006**, *11*, 17-28.
- (15) Marullo, N. P.; Mayfield, C. B.; Wagener, E. H. *J. Am. Chem. Soc.* **1968**, *90*, 510-511.
- (16) Fu, J.; Lau, K.; Barra, M. *J. Org. Chem.* **2009**, *74*, 1770-1773.
- (17) Vaughan, K.; Steven, M. F. G. *Chem. Soc. Rev.* **1978**, *7*, 377-397.
- (18) Moore, D. S.; Tobinson, S. D. *Adv. Inorg. Chem. Radiochem.* **1986**, *30*, 1-68.

- (19) Bräse, S.; Dahmen, S.; Lauterwasser, F.; Leadbeater, N. E.; Sharp, E. L. *Bioorg. Med. Chem. Lett.* **2002**, *12*, 1849-1851.
- (20) Nuricumbo-Escobar, J. J.; Campos-Alvarado, C.; Ríos-Moreno, G.; Morales-Morales, D.; Walsh, P. J.; Parra-Hake, M. *Inorg. Chem.* **2007**, *46*, 6182-6189.
- (21) Shiti, C.; Xu, L. *Talanta* **1992**, *39*, 1395-1398.
- (22) Das, B.; Shome, S. C. *Talanta* **1970**, *17*, 75-79.
- (23) Zhao, Y.; Cao, Q.-E.; Hu, Z.; Xu, Q. *Anal. Chim. Acta* **1999**, *388*, 45-50.
- (24) Gao, H.; Tao, M.; Wang, L. *Can. J. Anal. Sci. Spectrosc.* **1999**, *44*, 119-124.
- (25) Connelly, N. G.; Garcia, G. *J. Chem. Soc. Dalton Trans.* **1987**, *11*, 2737-2740.
- (26) Tejel, C.; Ciriano, M. A.; Ríos-Moreno, G.; Dobrinovitch, I. T.; Lahoz, F. J.; Oro, L. A.; Parra-Hake, M. *Inorg. Chem.* **2004**, *43*, 4719-4726.
- (27) Albertin, G.; Antoniutti, S.; Bedin, M.; Castro, J.; Garcia-Fontán, S. *Inorg. Chem.* **2006**, *45*, 3816-3825.
- (28) Brinckman, F. E.; Haiss, H. S.; Robb, R. A. *Inorg. Chem.* **1964**, 936-942.
- (29) Corbett, M.; Hoskins, B. F.; McLeod, N. J.; O'Day, B. P. *Aust. J. Chem.* **1975**, *28*, 2377-2392.
- (30) Ríos-Moreno, G.; Aguirre, G.; Parra-Hake, M.; Walsh, P. J. *Polyhedron* **2003**, *22*, 563-568.
- (31) Payehghadr, M.; Rofouei, M. K.; Morsali, A.; Shamsipur, M. *Inorg. Chim. Acta* **2007**, *360*, 1792-1798.
- (32) Yamada, H.; Ohta, H.; Yamaguchi, M.; Tsumaki, T. *Bull. Chem. Soc. Jpn.* **1960**, *34*, 214-243.

- (33) Ruiz, J.; López, J. F. J.; Rodríguez, V.; Pérez, J.; Ramírez de Arellano, M. C.; López, G. *J. Chem. Soc., Dalton Trans.* **2001**, 2683-2689.
- (34) Knowles, C. M.; Watt, G. W. *J. Am. Chem. Soc.* **1942**, *64*, 935-937.
- (35) Leman, J. T.; Barron, A. R.; Ziller, J. W.; Kren, R. M. *Polyhedron* **1989**, *8*, 1909-1912.
- (36) Kume, S.; Nishihara, H. *Strut. Bond* **2007**, *123*, 79-112.
- (37) Radu, A.; Scarmagnani, S.; Byrne, R.; Slater, C.; Lau, K. T.; Diamond, D. *J. Phys. D: Appl. Phys.* **2007**, *40*, 7238-7244.
- (38) Hardie, R. L.; Thomson, R. H. *J. Chem. Soc.* **1958**, 1286-1290.
- (39) Lippmaa, E.; Saluvere, T.; Pehk, T.; Olivson, A. *Org. Magn. Reson.* **1973**, *5*, 429-436.
- (40) Lippert, T.; Stebani, J.; Nuyke, O.; Stasko, A.; Wokaun, A. *J. Photochem. Photobiol. A: Chem.* **1994**, *78*, 139-148.
- (41) Urech, L.; Lippert, T.; Phipps, C. R.; Wokaun, A. *Appl. Surf. Sci.* **2007**, *253*, 6409-6415.
- (42) Lippert, T.; Dickson, J. T. *Chem. Rev.* **2003**, *103*, 453-485.
- (43) Smith, R. H., Jr.; Denlinger, C. L.; Kupper, R.; Mehl, A. F.; Michejda, C. J. *J. Am. Chem. Soc.* **1986**, *108*, 3726-3730.
- (44) Smith, R. H., Jr.; Wladkowski, B. D.; Herling, J. A.; Pfaltzgraff, T. D.; Pruski, B.; Klose, J.; Michejda, C. J. *J. Org. Chem.* **1992**, *57*, 654-661.
- (45) Schmidt, B. F.; Synder, E. J.; Carroll, R. M.; Farnsworth, D. W.; Michejda, C. J.; Smith, R. H., Jr. *J. Org. Chem.* **1997**, *62*, 8660-8665.

- (46) Nevěčná, T.; Pytela, O.; Ludwig, M.; Kaválek, J. *Collect. Czech. Chem. Commun.* **1990**, *55*, 147-155.
- (47) Pytela, O.; Nevěčná, T.; Kaválek, J. *Collect. Czech. Chem. Commun.* **1990**, *55*, 2701-2706.
- (48) Ludwig, M.; Kabickova, M. *Collect. Czech. Chem. Commun.* **1996**, *61*, 355-363.
- (49) Pytela, O.; Bednár, R.; Kaválek, J. *J. Phys. Org. Chem.* **2004**, *17*, 343-349.
- (50) Isaacs, N. *Physical Organic Chemistry*; 2nd ed.; Longman: New York, 1995; (a) Ch. 9; (b) Ch. 2; (c) Ch. 4.
- (51) Schmiedekamp, A.; Smith, R. H., Jr.; Michejda, C. J. *J. Org. Chem.* **1988**, *53*, 3433-3436.
- (52) Rakotondradany, F.; Williams, C. I.; Whitehead, M. A.; Jean-Claude, B. J. *J. Mol. Struct.* **2001**, *535*, 217-234.
- (53) Pytela, O.; Nevěčná, T.; Ludwig, M. *Collect. Czech. Chem. Commun.* **1990**, *55*, 156-164.
- (54) Kimball, D. B.; Haley, M. M. *Angew. Chem. Int. Ed.* **2002**, *41*, 3338-3351.
- (55) Lazny, R.; Sienkiewicz, M.; Bräse, S. *Tetrahedron* **2001**, *57*, 5825-5832.
- (56) Dahmen, S.; Bräse, S. *Angew. Chem. Int. Ed.* **2000**, *39*, 3681-3683.
- (57) Gross, M. L.; Blank, D. H.; Welch, W. M. *J. Org. Chem.* **1993**, *58*, 2104-2109.
- (58) Pages, T.; Langlois, B. R. *J. Fluorine Chem.* **2001**, *107*, 321-327.
- (59) Chu, C.-K.; Kim, J.-H.; Kim, D. W.; Chung, K.-H.; Katzenellenbogen, J. A.; Chi, D. Y. *Bull. Korean Chem. Soc.* **2005**, *26*, 599-602.
- (60) Hudson, J. L.; Jian, H.; Leonard, A. D.; Stephenson, J. J.; Tour, J. M. *Chem. Mater.* **2006**, *18*, 2766-2770.

- (61) Kolar, G. F. In *Chemical Carcinogens*; Searle, C. E., Ed.; ACS Press: Washington, D. C. , 1984; Vol. 2, Ch. 14.
- (62) Wilman, D. E. V. *Cancer Treat. Rev.* **1988**, *15*, 69-72.
- (63) Marchesi, F.; Turriziani, M.; Tortorelli, G.; Avvisati, G.; Torino, F.; De Vecchi, L. *Pharmacol. Res.* **2007**, *56*, 275-287.
- (64) Krois, D.; Brinker, U. H. In *Cyclodextrins and their Complexes*; Dodziuk, H., Ed.; Wiley: Weinheim, 2006; Ch. 10.4.
- (65) Szejtli, J. *Pure Appl. Chem.* **2004**, *76*, 1825-1845.
- (66) Takahashi, K.; Hattori, K.; Toda, F. *Tetrahedron Lett.* **1984**, *25*, 3331-3334.
- (67) Szejtli, J. *Chem. Rev.* **1998**, *98*, 1743-1754.
- (68) del Valle, E. M. M. *Process Biochem.* **2004**, *39*, 1033-1046.
- (69) Szejtli, J. In *Comprehensive Supramolecular Chemistry*; Pergamon: New York, 1996; Vol. 3, pp 1.
- (70) Bender, M. L.; Komiyama, M. *Cyclodextrin Chemistry*; Springer-Verlag: New York, 1978; (a) Ch. 4; (b) Ch. 5.
- (71) Cal, K.; Centkowska, K. *Eur. J. Pharm. Biopharm.* **2008**, *68*, 467-478.
- (72) Brewster, M. E.; Loftsson, T. *Adv. Drug Delivery Rev.* **2007**, *59*, 645-666.
- (73) Villalonga, R.; Cao, R.; Fragoso, A. *Chem. Rev.* **2007**, *107*, 3088-3116.
- (74) Hedges, A. R. *Chem. Rev.* **1998**, *98*, 2035-2044.
- (75) Schneiderman, E.; Stalcup, A. M. *J. Chromatogr. B* **2000**, *745*, 83-102.
- (76) VanEtten, R. L.; Clowes, G. A.; Sebastian, J. F.; Bender, M. L. *J. Am. Chem. Soc.* **1967**, *89*, 3253-3262.

- (77) VanEtten, R. L.; Sebastian, J. F.; Clowes, G. A.; Bender, M. L. *J. Am. Chem. Soc.* **1967**, *89*, 3242-3253.
- (78) Komiyama, M.; Bender, M. L. *J. Am. Chem. Soc.* **1978**, *100*, 2259-2260.
- (79) Marinescu, L. G.; Bols, M. *Angew. Chem., Int. Ed.* **2006**, *45*, 4590-4593.
- (80) Lopez, O. L.; Marinescu, L.; Bols, M. *Tetrahedron* **2007**, *63*, 8872-8880.
- (81) Sanchez, A. M.; de Rossi, R. H. *J. Org. Chem.* **1996**, *61*, 3446-3451.
- (82) García-Río, L.; Hall, R. W.; Mejuto, J. C.; Rodriguez-Dafonte, P. *Tetrahedron* **2007**, *63*, 2208-2214.
- (83) Iley, J.; Moreira, R.; Rosa, E. *J. Chem. Soc. Perkin Trans. II* **1991**, 81-85.
- (84) Silberberg, M. S. In *Principles of General Chemistry*; 1st ed.; Ed.; McGraw-Hill: New York, 2007, Ch. 22.
- (85) Harris, D. C. *Quantitative Chemical Analysis*; 4th ed.; Freeman: New York, 1995; Ch. 19.
- (86) Gil, V. M. S.; Oliveira, N. C. *J. Chem. Edu.* **1990**, *67*, 473-478.
- (87) Bruneau, E.; Lavabre, D.; Levy, G.; Micheau, J. C. *J. Chem. Edu.* **1992**, *69*, 833-837.
- (88) Párkányi, C.; Vernin, G.; Julliard, M.; Metzger, J. *Helv. Chim. Acta* **1981**, *64*, 171-175.
- (89) Preat, J.; Michaux, C.; Lewalle, A.; Perpète, E. A.; Jacquemin, D. *Chem. Phys. Lett.* **2008**, *451*, 37-42.
- (90) Chen, N. M.Sc., University of Waterloo, 2000, a) pp. 58-77; b) pp. 78-83.
- (91) Skoog, D. A.; Holler, F. J.; Nieman, T. A. *Principles of Instrumental Analysis*; 5th ed.; Saunders: Philadelphia, 1998; Ch. 14.

- (92) Connors, K. A. In *Binding Constants. The measurement of Molecular Complex Stability*; Wiley: New York, 1987; Ch. 4.
- (93) Harris, C. M.; Hoskins, B. F.; Martin, R. L. *J. Chem. Soc.* **1959**, 3728-36.
- (94) Cotton, F. A.; Wilkinson, G. In *Advanced Inorganic Chemistry*; Wiley: New York, 1988; pp. 942.
- (95) Handel, L. In *CRC Handbook of Organic Photochemistry*; Scaiano, J. C., Ed.; CRC Boca Raton, 1989; Vol. 1, pp. 279-287.
- (96) Ershova, T. V.; Rukhadze, E. G.; Terent'ev, A. P. *J. Gen. Chem. USSR (Engl. Transl.)* **1969**, 39, 59-62.
- (97) Reichardt, C. *Solvents and Solvent Effects in Organic Chemistry*; Wiley: Weinheim, 2003; a) Ch. 4; b) Ch. 5.
- (98) Petrucci, R. H.; Harwood, W. S.; Herring, F. G. *General Chemistry: Principles and Modern Applications*; 8th ed.; Prentice Hall: Upper Saddle River, 2002; Ch. 25.
- (99) Höner, M.; Broch, F.; do Canto Visentin, L. *Z. Anorg. Allg. Chem.* **2007**, 633, 1779-1782.
- (100) Guharoy, C.; Drew, M. G. B.; Bhattacharya, S. *J. Chem. Sci.* **2009**, 121, 257-266.
- (101) Kazitsyna, L. A.; Dzegilenko, N. B.; Upadysheva, A. V.; Mishchenko, V. V.; Reutov, O. A. *Izv. Akad. Nauk SSSR, Ser. Khim.* **1967**, 1925-1931.
- (102) Saunders, K. H.; Allen, R. L. M. In *Aromatic Diazo Compounds*; Edward Arnold: London, 1985, Ch. 6
- (103) Štefane, B.; Kočevár, M.; Polanc, S. *J. Org. Chem.* **1997**, 62, 7165-7169.
- (104) Sukigara, M.; Kikuchi, S. *Bull. Chem. Soc. Jpn.* **1967**, 40, 1077-1081.

- (105) Snatzke, G. In *Circular Dichroism: Principles and Applications*; Nakanishi, K., Berova, N., Woody, R., W., Eds.; Wiley: New York, 1994; Ch. 1.
- (106) González-Gaitano, G.; Rodríguez, P.; Isasi, J. R.; Fuentes, M.; Tardajos, G.; Sánchez, M. *J. Incl. Phenom. Macrocycl. Chem.* **2002**, *44*, 101-105.
- (107) *CRC Handbook of Chemistry and Physics*; Lide, D. R., Ed.; CRC Press: Boca Raton, 1996; a) 8-49; b) 8-52.
- (108) Zvěřina, V.; Remeš, M.; Diviš, J.; Marhold, J.; Matrka, M. *Collect. Czech. Chem. Commun.* **1973**, *38*, 251-256.
- (109) Beneš, J.; Beránek, V.; Zimprich, J.; Vetešník, P. *Collect. Czech. Chem. Commun.* **1977**, *42*, 702-710.
- (110) Svoboda, P.; Pytela, O.; Večeřa, M. *Collect. Czech. Chem. Commun.* **1986**, *51*, 553-563.
- (111) Connors, K. A. *Chem. Rev.* **1997**, *97*, 1325-1357.
- (112) Gadre, A.; Rüdiger, V.; Schneider, H.; Connors, K. A. *J. Pharm. Sci.* **1997**, *86*, 236-243.
- (113) Asadi, A. V.-Z.; Barra, M.; unpublished results.
- (114) Demirelli, H.; Köseoğlu, F. *J. Solution Chem.* **2004**, *33*, 1501-1515.
- (115) Immel, S.; Lichtenthaler, F. W. *Starch/Stärke* **1996**, *48*, 225-232.
- (116) Sueishi, Y.; Kasahara, M.; Inoue, M.; Matsueda, K. *J. Incl. Phenom. Macrocycl. Chem.* **2003**, *46*, 71-75.
- (117) Zhdanov, Y. A.; Alekseev, Y. E.; Kompantseva, E. V.; Vergeichik, E. N. *Russ. Chem. Rev.* **1992**, *61*, 563-575.
- (118) Harata, K. *Bioorg. Chem.* **1981**, *10*, 255-265.

- (119) Kajtár, M.; Horváth-Toró, C.; Kuthi, É.; Szejtli, J. *Acta Chim. Acad. Sci. Hung.* **1982**, *110*, 327-355.
- (120) Kodaka, M. *J. Am. Chem. Soc.* **1993**, *115*, 3702-3705.
- (121) Yoshida, N.; Yamaguchi, H.; Higashi, M. *J. Chem. Soc. Perkin Trans. II* **1994**, *12*, 2507-2513.
- (122) Liu, Y.; Zhao, Y.-L.; Chen, Y.; Guo, D.-S. *Org. Biomol. Chem.* **2005**, *3*, 584-591.
- (123) Liu, Y.; Zhao, Y.-L.; Zhang, H.-Y.; Fan, Z.; Wen, G.-D.; Ding, F. *J. Phys. Chem.* **2004**, *108*, 8836-8843.
- (124) Suzuki, M.; Kajtár, M.; Szejtli, J.; Vikmon, M.; Fenyvesi, E. *Carbohydr. Res.* **1992**, *223*, 71-80.
- (125) Shi, J.; Guo, D.-S.; Ding, F.; Liu, Y. *Eur. J. Org. Chem.* **2009**, 923-931.
- (126) Connors, K. A.; Mulski, M. J.; Paulson, A. *J. Org. Chem.* **1992**, *57*, 1794-1798.
- (127) Cartwright, R. A.; Tatlow, J. C. *J. Chem. Soc.* **1953**, 1994-1998.
- (128) Vernin, G.; Siv, C.; Metzger, J.; Parkanyi, C. *Synthesis* **1977**, *10*, 691-693.
- (129) Baro, J.; Dudek, D.; Luther, K.; Troe, J. *Ber. Bunsenges. Phys. Chem.* **1983**, *87*, 1161-1164.
- (130) Harned, H. S.; Owen, B. B. In *The Physical Chemistry of Electrolytic Solutions*; 3rd ed.; Reinhold Publishing: New York, 1958, (a) 748 (b) 719.

Appendix. Observed rate constants for acid-catalyzed decomposition of 1,3-diphenyltriazenes in aqueous solutions

Table A-1. HDPT and CH₃ODPT in phosphate buffer.^a

pH ^b	$k_{\text{obs}} (10^{-4} \text{ s}^{-1})^{\text{b}}$	pH ^c	$k_{\text{obs}} (10^{-4} \text{ s}^{-1})^{\text{c}}$
6.76	3.8 ± 0.1	7.45	2.36 ± 0.01
6.46	7.1 ± 0.1	6.76	11.6 ± 0.4
6.28	9.60 ± 0.06	6.46	25 ± 1
6.16	12.6 ± 0.1	6.28	39 ± 2
		6.16	49 ± 3

^aIn 2% (v/v) MeOH/water, $\mu = 0.5 \text{ M}$ (NaCl), $T = 21 \text{ }^{\circ}\text{C}$. Observed rate constant values correspond to the average of two to four independent runs. ^bData for HDPT. ^cData for CH₃ODPT.

Table A-2. CH₃ODPT in the presence of β -CD in phosphate buffer at various pHs.^a

BCD (mM)	$k_{\text{obs}} (10^{-4} \text{ s}^{-1})$				
	pH = 6.51	pH = 6.69	pH = 6.80	pH = 7.07	pH = 7.46
none	280 ± 9	186 ± 2	138 ± 2	66.3 ± 0.5	26.2 ± 0.2
0.25	191 ± 7	131 ± 6	88 ± 2	46.6 ± 0.9	19.0 ± 0.1
0.50	169 ± 9	92 ± 3	68 ± 2	32.6 ± 0.2	14.1 ± 0.3
1.0	97 ± 7	57.2 ± 0.2	47 ± 1	22.9 ± 0.2	10.0 ± 0.1
2.0	64.4 ± 0.8	40.8 ± 0.2	30 ± 1	14.6 ± 0.4	6.14 ± 0.01
4.0	41.8 ± 0.6	24.7 ± 0.3	18.7 ± 0.1	9.1 ± 0.1	4.02 ± 0.01
6.0	29.9 ± 0.5	18.9 ± 0.5	14.3 ± 0.1	7.12 ± 0.06	3.30 ± 0.02
8.0	24.0 ± 0.4	15.7 ± 0.2	12.2 ± 0.2	5.99 ± 0.02	2.76 ± 0.01
11	20.6 ± 0.5	13.4 ± 0.1	10.0 ± 0.1	4.96 ± 0.02	2.28 ± 0.01
14	17.6 ± 0.2	11.7 ± 0.1	8.82 ± 0.04	4.44 ± 0.003	1.96 ± 0.08

^aIn 2% (v/v) MeOH/water, $\mu = 0.55 \text{ M}$ (NaCl), $T = 21 \text{ }^{\circ}\text{C}$. Observed rate constant values correspond to the average of two to four independent runs.

Table A-3. HDPT in the presence of different CDs varying in concentration in phosphate buffer at pH 6.16.^a

CD (mM)	$k_{\text{obs}}/10^{-4} \text{ s}^{-1}$			
	α -CD	β -CD	HP- β -CD	TM- β -CD
none	12.7 ± 0.1	12.5 ± 0.2	12.5 ± 0.2	12.6 ± 0.1
0.10			9.7 ± 0.1	
0.20	10.9 ± 0.2	10.6 ± 0.1 ^b	7.70 ± 0.04	10.2 ± 0.1 ^b
0.50	9.22 ± 0.09	9.0 ± 0.1	4.84 ± 0.02	8.4 ± 0.2
1.0	7.20 ± 0.03	6.70 ± 0.06	2.80 ± 0.01	6.10 ± 0.01
2.0	4.92 ± 0.01	4.94 ± 0.02	1.61 ± 0.01	3.88 ± 0.05
3.0	3.54 ± 0.04			
4.0	2.82 ± 0.02	3.26 ± 0.01	0.925 ± 0.008	2.28 ± 0.01 ^c
6.0	2.2 ± 0.1 ^d	2.58 ± 0.02		
7.0	1.59 ± 0.01	2.22 ± 0.03 ^e	0.582 ± 0.006	1.32 ± 0.02
10	1.17 ± 0.02	1.88 ± 0.01 ^f	0.452 ± 0.001	0.908 ± 0.002
14		1.64 ± 0.01	0.330 ± 0.002	0.64 ± 0.01

^a In 2% (v/v) MeOH/water, $\mu = 0.5 \text{ M}$ (NaCl), $T = 21 \text{ }^\circ\text{C}$. Observed rate constant values correspond to the average of two to four independent runs. ^b 0.25 mM. ^c 4.3 mM. ^d 5.5 mM. ^e 8.0 mM. ^f 11 mM.

Table A-4. CH₃ODPT in the presence of different CDs varying in concentration in phosphate buffer at pH 6.16.^a

CD (mM)	$k_{\text{obs}}/10^{-3} \text{ s}^{-1}$			
	α -CD	β -CD	HP- β -CD	TM- β -CD
none	52 ± 1	50.6 ± 0.4	48.9 ± 0.2	46 ± 3
0.10	43 ± 1		28.6 ± 0.1	
0.20	39.1 ± 0.4	29.2 ± 0.2 ^b	19.2 ± 0.1	31 ± 1 ^b
0.50	28 ± 1	22 ± 2	9.8 ± 0.3	23 ± 2
1.0	15.9 ± 0.1	14 ± 1	4.96 ± 0.01	13.2 ± 0.3
2.0	7.5 ± 0.1	7.7 ± 0.1	2.72 ± 0.01	7.6 ± 0.1
4.0	2.38 ± 0.02	4.79 ± 0.09	1.74 ± 0.02	3.7 ± 0.1
6.0		3.76 ± 0.04		
7.0	0.880 ± 0.001	3.38 ± 0.06 ^c	1.03 ± 0.005	2.1 ± 0.1
10	0.41 ± 0.01	2.80 ± 0.02	0.800 ± 0.003	1.51 ± 0.05
14		2.5 ± 0.1	0.632 ± 0.007	0.98 ± 0.02

^a In 2% (v/v) MeOH/water, $\mu = 0.5 \text{ M}$ (NaCl), $T = 21 \text{ }^\circ\text{C}$. Observed rate constant values correspond to the average of two to four independent runs. ^b 0.25 mM. ^c 8.0 mM.